

Broken symmetry states in bilayer graphene in electric and in-plane magnetic fields

Junji Jia,¹ P. K. Pyatkovskiy,² E. V. Gorbar,^{3,4} and V. P. Gusynin⁴

¹*School of Physics and Technology, and MOE Key Laboratory of Artificial Micro- and Nano-structures, Wuhan University, 430072, China*

²*Department of Physics and Astronomy, University of Manitoba, Winnipeg, MB R3T 2N2, Canada*

³*Department of Physics, Taras Shevchenko National Kiev University, 03022, Kiev, Ukraine*

⁴*Bogolyubov Institute for Theoretical Physics, 03680, Kiev, Ukraine*

(Dated: September 23, 2018)

Broken symmetry states in bilayer graphene in perpendicular electric E_{\perp} and in-plane magnetic B_{\parallel} fields are studied in the presence of the dynamically screened long-range Coulomb interaction and the symmetry-breaking contact four-fermion interactions. The integral gap equations are solved numerically, and it is shown that the momentum dependence of gaps is essential: It diminishes by an order of magnitude the gaps compared to the case of momentum-independent approximation, and the obtained gap magnitudes are found to agree well with existing experimental values. We derived a phase diagram of bilayer graphene at the neutrality point in the plane $(B_{\parallel}, E_{\perp})$ showing that the (canted) layer antiferromagnetic (LAF) state remains a stable ground state of the system at large B_{\parallel} . On the other hand, while the LAF phase is realized at small values of E_{\perp} , the quantum valley Hall (QVH) phase is the ground state of the system at values $E_{\perp} > E_{cr}(B_{\parallel})$, where a critical value $E_{cr}(B_{\parallel})$ increases with in-plane magnetic field B_{\parallel} .

I. INTRODUCTION

The interlayer hopping γ_1 in Bernal stacked bilayer graphene modifies [1] the linear Dirac-type spectrum of charge carriers realized at high energy to the quadratic spectrum at low energy. Quasiparticles in bilayer graphene are gapless and are characterized by the particle-hole symmetric parabolic conduction and valence bands with massive chiral charge carriers, touching at two K and K' valley points. The crossover between the linear Dirac and quadratic dispersion takes place at energy $E \simeq \gamma_1/4$.

The quadratic spectrum in bilayer graphene immediately implies [2] that the electron-electron interaction should open a gap in the spectrum at the neutrality point in clean bilayer samples. The corresponding reasoning is straightforward. Since the electron density of states vanishes at the Dirac points in monolayer graphene, the condensate of electron-hole pairs and the quasiparticle gap are formed only when the coupling constant exceeds a certain critical value [3–7]. In this case the condensate and gap acquire the exponential Berezinsky-Kosterlitz-Thouless-like behavior with respect to the coupling constant. On the other hand, the density of states for the quadratic spectrum is nonzero and a gap in bilayer graphene is generated for an arbitrary small interaction and has the exponential Bardeen-Cooper-Schrieffer-like behavior for static screening, and the gap has a power-law scaling in the coupling strength for the dynamically screened Coulomb interaction [8, 9]. These theoretical considerations are confirmed by the experimental data, where no sign of an insulating state [10] down to 1 K and gaps [11–14] of order 5–25 K are observed in monolayer and bilayer graphene, respectively, in the absence of external electromagnetic fields.

In this connection, we note that in the presence of a strong perpendicular magnetic field the kinetic energy is quenched on the lowest Landau level and the quasiparticle band is completely flat. This leads to the gap generation at any small coupling in monolayer graphene [3, 15, 16] and enhancement of gaps in bilayer graphene.

The low-energy electron Hamiltonian with the Coulomb interaction in bilayer graphene possesses the approximate spin-valley SU(4) symmetry. This opens many interesting possibilities for the choice of an order parameter. For example, in the absence of electromagnetic fields, the quantum anomalous Hall (QAH) [17, 18], the quantum spin Hall (QSH), and the layer antiferromagnet states were suggested as possible gapped ground states of bilayer graphene at the neutrality point (for a general discussion, see Ref. [19]). The QAH and QSH state gaps are due to the Haldane mass [20] symmetric and antisymmetric in spin, respectively. The LAF state gap is described by the Dirac mass antisymmetric in spin whereas the quantum valley Hall state gap is described by the Dirac mass symmetric in spin.

Experimentally, the broken symmetry states in bilayer graphene were studied in the presence of a rather strong perpendicular magnetic field in Refs. [11–13, 21–26], where it was found that the eightfold degeneracy in the zero-energy Landau level can be lifted completely, giving rise to the quantum Hall states with filling factors $\nu = 0, \pm 1, \pm 2, \pm 3$. These states have been investigated theoretically in Refs. [8, 27–36] and a reasonable agreement with the experimental data was found. However, the nature of the ground state of bilayer graphene in the absence or weak out-of-plane component of a magnetic field remains a matter of debate.

Since the SU(4) symmetry is approximate in bilayer graphene, the role of the interaction terms in the Hamiltonian which break this symmetry is crucially important. The valley-asymmetric interactions, which arise from the Coulomb

interactions at the lattice scale or electron-phonon interactions with the optical phonon modes, were considered in Refs. [27, 37–40]. Taking these interactions into account and using the experimental data as a guide, the canted antiferromagnetic (CAF) state was suggested as the ground state in both monolayer [41] and bilayer graphene [27, 37, 38] at the neutrality point in a magnetic field.

The existing studies of the CAF state [27, 37, 38] considered a model with only local four-fermion interactions where in the mean-field approximation the gap equations are algebraic and generated gaps are constant. It is well known that the long-range Coulomb interaction does not permit constant gaps as solutions of integral gap equations, and momentum-dependent gaps have essentially smaller magnitude (see, for example, Ref. [5]). Therefore, it is important to investigate the ground state in bilayer graphene when both the long-range Coulomb interaction and the SU(4) symmetry-breaking local interactions are present. In addition, experimental studies of bilayer graphene in external fields of different orientation have become available recently [42, 43]. This provides the motivation for the study of the broken symmetry states in bilayer graphene at the neutrality point in the present paper, where we pay special attention to the role of the long-range Coulomb interaction as well as perpendicular electric and parallel magnetic fields on the broken symmetry states in bilayer graphene. Furthermore, we consider the case of a weak perpendicular magnetic field treating it as a parameter of the perturbative expansion.

The paper is organized as follows. We begin by presenting in Sec. II the model describing low-energy quasiparticle excitations in bilayer graphene in an external magnetic field interacting by means of the long-range Coulomb interaction and the local four-fermion interactions. The gap equations are derived in Sec. III and analyzed in electric and in-plane magnetic fields in Sec. IV in the case where out-of-plane magnetic field B_\perp is absent. Solutions in in-plane magnetic field are found in Sec. V. The linear and quadratic in B_\perp corrections to the gap equation are considered in Sec. VI. The results obtained in the paper are summarized and discussed in Sec. VII. In Appendix A, the gap equations for the momentum-dependent generalized chemical potentials and gaps are derived. The gap equations in the second order in B_\perp are written down in Appendix B.

II. MODEL

We utilize the same model for describing the low-energy electronic excitations as in Refs. [32, 35, 36]. The free part of the effective low-energy Hamiltonian of bilayer graphene reads

$$H_0 = -\frac{1}{2m_*} \sum_{\xi,s} \int d^2\mathbf{r} \Psi_{\xi s}^\dagger(\mathbf{r}) \begin{pmatrix} 0 & (\pi^\dagger)^2 \\ \pi^2 & 0 \end{pmatrix} \Psi_{\xi s}(\mathbf{r}), \quad (1)$$

where $\pi = \hat{p}_x + i\hat{p}_y$ and the canonical momentum $\hat{\mathbf{p}} = -i\hbar\nabla + e\mathbf{A}/c$ includes the vector potential \mathbf{A} corresponding to the component of an external magnetic field \mathbf{B}_\perp perpendicular to the bilayer planes. The quasiparticle mass is $m_* = \gamma_1/2v_F^2 \approx 0.054m_e$, where $v_F \approx 8.0 \times 10^5$ m/s is the Fermi velocity, $\gamma_1 \approx 0.39$ eV, and m_e is the mass of the electron. The two-component spinor field $\Psi_{\xi s}$ carries the valley ($\xi = K, K'$) and spin ($s = \pm 1$) indices. We use the standard convention [1]: $\Psi_{Ks}^T = (\psi_{KA_1}, \psi_{KB_2})_s$ for valley K and $\Psi_{K's}^T = (\psi_{K'B_2}, \psi_{K'A_1})_s$ for valley K' . Indices A_1 and B_2 label the corresponding A and B sublattices in the layers 1 (top) and 2 (bottom), respectively, which, according to the Bernal ($A_2 - B_1$) stacking, are relevant for the low-energy dynamics.

The Zeeman and Coulomb interactions plus the top-bottom gates voltage imbalance m_0 (we denote it m_0 because it corresponds to the time-reversal invariant bare Dirac mass) in bilayer graphene are described as follows:

$$H_{\text{int}} = \int d^2\mathbf{r} \Psi^\dagger(\mathbf{r}) [\mu_B \boldsymbol{\sigma} \mathbf{B} + m_0 \eta_3 \tau_3] \Psi(\mathbf{r}) + \frac{1}{2} \int d^2\mathbf{r} d^2\mathbf{r}' \left\{ V(\mathbf{r} - \mathbf{r}') \rho(\mathbf{r}) \rho(\mathbf{r}') + 2V_{\text{IL}}(\mathbf{r} - \mathbf{r}') \rho_1(\mathbf{r}) \rho_2(\mathbf{r}') \right\}, \quad (2)$$

where Ψ combines the fields Ψ_{Ks} and $\Psi_{K's}$ into an eight-component spinor. Here μ_B is the Bohr magneton, $\mathbf{B} = \mathbf{B}_\perp + \mathbf{B}_\parallel$ is the total magnetic field with component \mathbf{B}_\parallel parallel to the bilayer planes, σ_i are Pauli matrices in spin space, η_3 is the third Pauli matrix acting on the valley index of the fermion field, and τ_3 is the diagonal Pauli matrix acting on the two components of the fields Ψ_{Ks} and $\Psi_{K's}$. Note that the presence of η_3 in the voltage imbalance term is related to the different order of the A_1 and B_2 components in Ψ_{Ks} and $\Psi_{K's}$. The bias voltage between the top and bottom gates is related to the electric field E_\perp applied perpendicularly to the bilayer planes: $m_0 = eE_\perp d/2$, where $d = 3.5 \times 10^{-10}$ m is the distance between the layers. In our model, the in-plane component of B_\parallel enters only through the Zeeman term, and we neglect its orbital effects due to finite d , which modify the electron spectrum [44–47] at energies smaller than the trigonal warping scale of about 1 meV [1] even at highest accessible fields.

The Coulomb interaction term $V(\mathbf{r}) = e^2/(\kappa|\mathbf{r}|)$ in H_{int} is the bare intralayer potential whose Fourier transform is given by $V(p) = 2\pi e^2/(\kappa p)$, where κ is the dielectric constant. The Fourier transform of the interaction $V_{\text{IL}}(\mathbf{r})$ equals $V_{\text{IL}}(p) = 2\pi e^2(e^{-pd} - 1)/(\kappa p)$. The interaction $V_{\text{IL}}(\mathbf{r}) = e^2/(\kappa\sqrt{\mathbf{r}^2 + d^2}) - V(\mathbf{r})$ describes the d -dependent part of

the interlayer electron interactions and unlike the Coulomb interaction is not invariant with respect to the spin-valley SU(4) symmetry. Since d is small in bilayer graphene, this interaction is weak. The two-dimensional charge densities in the two layers are (the total charge density $\rho = \rho_1 + \rho_2$)

$$\rho_1(\mathbf{r}) = \Psi^\dagger(\mathbf{r})\mathcal{P}_1\Psi(\mathbf{r}), \quad \rho_2(\mathbf{r}) = \Psi^\dagger(\mathbf{r})\mathcal{P}_2\Psi(\mathbf{r}), \quad (3)$$

where $\mathcal{P}_1 = (1 + \eta_3\tau_3)/2$ and $\mathcal{P}_2 = (1 - \eta_3\tau_3)/2$ are projectors on the states in the layers 1 and 2, respectively. When the dynamical screening effects are taken into account, the potentials $V(\mathbf{r})$ and $V_{\text{IL}}(\mathbf{r})$ are replaced by effective interactions $V_{\text{eff}}(t, \mathbf{r})$ and $V_{\text{IL}}^{\text{eff}}(t, \mathbf{r})$ which are no longer instantaneous.

If external electric and magnetic fields are absent and the interaction V_{IL} is neglected, then the Hamiltonian $H = H_0 + H_{\text{int}}$, with H_0 and H_{int} in Eqs. (1) and (2), possesses the spin-valley SU(4) symmetry and all the QAH, QVH, QSH, and LAF states discussed in the Introduction are degenerate in energy at the neutrality point. In order to qualify these states, we write down their order parameters (condensates) in terms of the valley-layer components of the spinor Ψ :

$$\text{QAH:} \quad \langle \Psi^\dagger \tau_3 \Psi \rangle = \langle \psi_{KA_1s}^\dagger \psi_{KA_1s} - \psi_{K'A_1s}^\dagger \psi_{K'A_1s} - \psi_{KB_2s}^\dagger \psi_{KB_2s} + \psi_{K'B_2s}^\dagger \psi_{K'B_2s} \rangle, \quad (4)$$

$$\text{QVH:} \quad \langle \Psi^\dagger \eta_3 \tau_3 \Psi \rangle = \langle \psi_{KA_1s}^\dagger \psi_{KA_1s} + \psi_{K'A_1s}^\dagger \psi_{K'A_1s} - \psi_{KB_2s}^\dagger \psi_{KB_2s} - \psi_{K'B_2s}^\dagger \psi_{K'B_2s} \rangle, \quad (5)$$

$$\text{QSH:} \quad \langle \Psi^\dagger \sigma_3 \tau_3 \Psi \rangle = \langle \psi_{KA_1s}^\dagger s \psi_{KA_1s} - \psi_{K'A_1s}^\dagger s \psi_{K'A_1s} - \psi_{KB_2s}^\dagger s \psi_{KB_2s} + \psi_{K'B_2s}^\dagger s \psi_{K'B_2s} \rangle, \quad (6)$$

$$\text{LAF:} \quad \langle \Psi^\dagger \sigma_3 \eta_3 \tau_3 \Psi \rangle = \langle \psi_{KA_1s}^\dagger s \psi_{KA_1s} + \psi_{K'A_1s}^\dagger s \psi_{K'A_1s} - \psi_{KB_2s}^\dagger s \psi_{KB_2s} - \psi_{K'B_2s}^\dagger s \psi_{K'B_2s} \rangle, \quad (7)$$

where the summation over the spin index is implied. The QAH state describes a state in which the K and K' valleys have opposite layer polarizations leading to the quantum Hall effect even in the absence of a magnetic field. For the QVH state, the layer polarization is the same for both valleys, breaking thus an inversion symmetry; therefore, this state can be called also a layer-polarized state. The QSH and LAF states at fixed spin have the same order parameter as the QAH and QVH states and, unlike the latter states, flip the sign of order parameter for the opposite direction of spin. Thus, the states QAH, QVH and QSH, LAF are symmetric and antisymmetric in spin, respectively. It is important to emphasize that the QVH and LAF states do not have topologically protected edge states and finite Hall conductivities, while the QAH and QSH states possess topologically protected edge states leading to nonzero charge and spin Hall conductivities, respectively [18, 19]. The time-reversal symmetry is unbroken for the QVH, QSH and broken for QAH, LAF states. Since at the neutrality point $\rho = \rho_1 + \rho_2 = 0$, the negative interaction term V_{IL} in Hamiltonian (2) makes the layer-polarized QVH state have larger energy than the other three QAH, QSH, and LAF states, which remain degenerate in energy.

Clearly, for a sufficiently large electric field E_\perp perpendicular to the planes of graphene, the layer-polarized QVH state should be realized. The experiments performed in Refs. [11, 12] demonstrated a phase transition to another state as E_\perp decreases. This eliminates the QVH state as a possible candidate for the ground state of bilayer graphene at the neutrality point in the absence of external fields. On the other hand, the recent experiment [42] revealed a quantum phase transition at large in-plane magnetic field to a state with the conductance of order $4e^2/h$ consistent with the QSH state. This also excludes the QSH state as the ground state of bilayer graphene in the absence of in-plane magnetic field. Since the QAH state has topologically protected edge states, hence nonzero conductance, the experimental data in Ref. [42] single out the insulating LAF phase as the ground state of bilayer graphene in the absence of external electric and in-plane magnetic fields. According to Refs. [27, 37], the LAF state transforms in an out-of-plane magnetic field into the CAF state once the Zeeman coupling is taken into account. Moreover, for $\mathbf{B}_\perp \neq 0$, the CAF state continuously crosses over into the QSH state as in-plane magnetic field increases.

Since the QAH, QSH, and LAF states are degenerate in energy for the Hamiltonian $H = H_0 + H_{\text{int}}$ with the long-range Coulomb interaction in the absence of external fields, new terms breaking the SU(4) symmetry should be added to the Hamiltonian in order to ensure that the LAF is the ground state of bilayer graphene. To provide this, the following local four-fermion interaction terms allowed by the symmetry of the bilayer lattice were added to the Hamiltonian of the model in Refs. [27, 37, 39]:

$$H_{\text{asym}} = \frac{2\pi\hbar^2}{m_*} \sum_{\alpha, \beta=0}^3 g_{\alpha\beta} \int d^2\mathbf{r} [\Psi^\dagger(\mathbf{r})\eta_\alpha\tau_\beta\Psi(\mathbf{r})]^2, \quad (8)$$

where η_j are the Pauli matrices acting on the valley degree of freedom of the fermion field and we set the SU(4)-symmetric coupling constant g_{00} of the local Coulomb interaction to zero. As argued in Refs. [37, 38, 41], the U(4)-asymmetric interactions (8) arise actually from the Coulomb interaction at the lattice scale $a \approx 2.46 \text{ \AA}$ or electron-phonon interactions with the optical phonon modes, therefore, they can be assumed to be local in the effective low-energy model. There are generically eight independent dimensionless coupling constants $g_{\perp\perp} \equiv g_{11} = g_{12} = g_{21} = g_{22}$,

$g_{\perp 0} \equiv g_{10} = g_{20}$, $g_{0\perp} \equiv g_{01} = g_{02}$, $g_{\perp z} \equiv g_{13} = g_{23}$, $g_{z\perp} \equiv g_{31} = g_{32}$, $g_{zz} \equiv g_{33}$, $g_{z0} \equiv g_{30}$, and $g_{0z} \equiv g_{03}$, whose bare values should be less or order of the dimensionless strength of the Coulomb interaction at the lattice scale $e^2 am_*/\hbar^2 \approx 0.25$. As we will see, not all local couplings $g_{\alpha\beta}$ are relevant for determining the phase diagram of the system, and only certain combinations of them are important.

III. GAP EQUATION

The Schwinger–Dyson (SD) or gap equation for the quasiparticle Green’s function (propagator) in the Hartree-Fock approximation reads [32, 36]

$$\begin{aligned} G^{-1}(x, y) &= S^{-1}(x, y) - (\mu_B \boldsymbol{\sigma} \mathbf{B} + m_0 \eta_3 \tau_3) \delta^3(x - y) - iG(x, y) V_{\text{eff}}(x - y) \\ &- i[\mathcal{P}_1 G(x, y) \mathcal{P}_2 + \mathcal{P}_2 G(x, y) \mathcal{P}_1] V_{\text{IL}}^{\text{eff}}(x - y) - i \frac{4\pi\hbar^2}{m_*} \sum_{\alpha, \beta=0}^3 g_{\alpha\beta} \eta_\alpha \tau_\beta G(x, x) \eta_\alpha \tau_\beta \delta^3(x - y) \\ &- \frac{i}{2} [\mathcal{P}_1 - \mathcal{P}_2] \text{tr}\{(\mathcal{P}_1 - \mathcal{P}_2) G(x, x)\} V_{\text{IL}}(0) \delta^3(x - y) + i \frac{4\pi\hbar^2}{m_*} \sum_{\alpha, \beta=0}^3 g_{\alpha\beta} \eta_\alpha \tau_\beta \text{tr}\{\eta_\alpha \tau_\beta G(x, x)\} \delta^3(x - y), \end{aligned} \quad (9)$$

where $x = (t, \mathbf{x})$, $G(x, y) = \hbar^{-1} \langle 0 | \Psi(x) \Psi^\dagger(y) | 0 \rangle$ is the full propagator, $S(x, y)$ is the free propagator in the theory with $m_0 = \mu_B |\mathbf{B}| = 0$, and $V_{\text{IL}}(0) = -2\pi e^2 d/\kappa$ is the Fourier transform of the interlayer interaction $V_{\text{IL}}(\mathbf{r})$ at zero momentum. Note also that due to the overall neutrality of the system, we dropped all Hartree terms proportional to $\text{tr}[G(x, x)]$ (i.e., the charge density) in the gap equation. The explicit form of the interlayer potential in momentum space $V_{\text{IL}}^{\text{eff}}(\omega, p)$ can be found in the Appendix of the second paper in Ref. [32]. Here we do not need it: Due to the presence of the projectors \mathcal{P}_1 and \mathcal{P}_2 in the second line of Eq. (9), the corresponding Fock term does not contribute to the final form of the gap equation if the Green’s functions are diagonal in the valley space. As to the effective interaction V_{eff} , in momentum space it reads

$$V_{\text{eff}}(\omega, p) = \frac{2\pi e^2}{\kappa} \frac{1}{p + \frac{\pi e^2}{\kappa} \Pi(\omega, p, \Delta_{\alpha\beta})}, \quad (10)$$

where $\Pi(\omega, p, \Delta_{\alpha\beta})$ is the polarization function. The one-loop polarization function $\Pi(\omega, p, \Delta_{\alpha\beta})$ as an integral over momentum is given in Ref. [17]. In this work, we will set quasiparticle gaps $\Delta_{\alpha\beta}$ to zero in the polarization function because it weakly depends on gaps. In this case, the polarization function is given by [8]:

$$\Pi(\omega, k) = \frac{4m_*}{\pi\hbar^2} P\left(\frac{\omega}{k}\right), \quad P(z) = \ln\left(\frac{4 + 4z^2}{1 + 4z^2}\right) + \frac{2 \arctan(z) - \arctan(2z)}{z}. \quad (11)$$

It is convenient to define the full quasiparticle propagator G through the self-energy Σ as follows:

$$G^{-1}(x, z) = S^{-1}(x, z) + \Sigma(x, z), \quad (12)$$

where $S^{-1}(x, z)$ is the free inverse propagator. Then the Schwinger–Dyson equation in terms of the self-energy takes the following form:

$$\begin{aligned} \Sigma(x, y) &= -(\mu_B \boldsymbol{\sigma} \mathbf{B} + m_0 \eta_3 \tau_3) \delta^3(x - y) - iG(x, y) V_{\text{eff}}(x - y) - i \frac{4\pi\hbar^2}{m_*} \sum_{\alpha, \beta=0}^3 g_{\alpha\beta} \eta_\alpha \tau_\beta G(x, x) \eta_\alpha \tau_\beta \delta^3(x - y) \\ &- i[\mathcal{P}_1 G(x, y) \mathcal{P}_2 + \mathcal{P}_2 G(x, y) \mathcal{P}_1] V_{\text{IL}}^{\text{eff}}(x - y) - \frac{i}{2} [\mathcal{P}_1 - \mathcal{P}_2] \text{tr}\{(\mathcal{P}_1 - \mathcal{P}_2) G(x, x)\} V_{\text{IL}}(0) \delta^3(x - y) \\ &+ i \frac{4\pi\hbar^2}{m_*} \sum_{\alpha, \beta=0}^3 g_{\alpha\beta} \eta_\alpha \tau_\beta \text{tr}\{\eta_\alpha \tau_\beta G(x, x)\} \delta^3(x - y). \end{aligned} \quad (13)$$

Although the quasiparticle propagator is not translation invariant when an out-of-plane magnetic field is present, it can be written in the form of the product of the non-translation-invariant Schwinger phase $\Phi(x, y) = -(e/\hbar c) \mathbf{x} \mathbf{A}(y)$ in the symmetric gauge $\mathbf{A} = (-B_\perp x_2/2, B_\perp x_1/2)$ and a translation invariant function

$$G(x, y) = e^{i\Phi(x, y)} \tilde{G}(x - y).$$

Then in terms of translation invariant self-energy $\tilde{\Sigma}(x-y) = \exp[-i\Phi(x,y)]\Sigma(x,y)$ and propagator $\tilde{G}(x-y)$, Eq. (13) takes the following form in momentum space:

$$\begin{aligned} \tilde{\Sigma}(\Omega, \mathbf{p}) &= -\mu_B \boldsymbol{\sigma} \mathbf{B} - m_0 \eta_3 \tau_3 - i \int \frac{d\omega d^2k}{(2\pi)^3} \tilde{G}(\omega, \mathbf{k}) V_{\text{eff}}(\Omega - \omega, \mathbf{p} - \mathbf{k}) \\ &- i \int \frac{d\omega d^2k}{(2\pi)^3} \left(\mathcal{P}_1 \tilde{G}(\omega, \mathbf{k}) \mathcal{P}_2 + \mathcal{P}_2 \tilde{G}(\omega, \mathbf{k}) \mathcal{P}_1 \right) V_{\text{IL}}(\Omega - \omega, \mathbf{p} - \mathbf{k}) - i \frac{4\pi\hbar^2}{m_*} \sum_{\alpha, \beta=0}^3 g_{\alpha\beta} \int \frac{d\omega d^2k}{(2\pi)^3} \eta_\alpha \tau_\beta \tilde{G}(\omega, \mathbf{k}) \eta_\alpha \tau_\beta \\ &- \frac{i}{2} \int \frac{d\omega d^2k}{(2\pi)^3} (\mathcal{P}_1 - \mathcal{P}_2) \text{tr} [(\mathcal{P}_1 - \mathcal{P}_2) \tilde{G}(\omega, \mathbf{k})] V_{\text{IL}}(0) + i \frac{4\pi\hbar^2}{m_*} \sum_{\alpha, \beta=0}^3 g_{\alpha\beta} \int \frac{d\omega d^2k}{(2\pi)^3} \eta_\alpha \tau_\beta \text{tr} \{ \eta_\alpha \tau_\beta \tilde{G}(\omega, \mathbf{k}) \}. \end{aligned} \quad (14)$$

Finally, in order to finish the setup of our problem, we should select an ansatz for the quasiparticle self-energy $\tilde{\Sigma}$. Since we consider the out-of-plane magnetic field \mathbf{B}_\perp in perturbation theory, we use the following ansatz for the self-energy up to the second order in \mathbf{B}_\perp :

$$\begin{aligned} \tilde{\Sigma}(\Omega, p) &= -\Delta_{\alpha\beta}(\Omega, p) \eta_\alpha \sigma_\beta \tau_3 - \mu_{\alpha\beta}(\Omega, p) \eta_\alpha \sigma_\beta - \mu_{\alpha\beta}^{(1)}(\Omega, p) \eta_\alpha \sigma_\beta B_\perp \\ &- \Delta_{\alpha\beta}^{(1)}(\Omega, p) \eta_\alpha \sigma_\beta \tau_3 B_\perp - \mu_{\alpha\beta}^{(2)}(\Omega, p) \eta_\alpha \sigma_\beta B_\perp^2 - \Delta_{\alpha\beta}^{(2)}(\Omega, p) \eta_\alpha \sigma_\beta \tau_3 B_\perp^2. \end{aligned} \quad (15)$$

The symmetry-breaking quantities $\mu_{\alpha\beta}(p)$ and $\Delta_{\alpha\beta}(p)$ are related to the corresponding order parameters through the following relationship:

$$\langle \Psi^\dagger \mathcal{O}^{\alpha\beta} \Psi \rangle = -\hbar \text{tr} [\mathcal{O}^{\alpha\beta} G(x, x)], \quad \langle \Psi^\dagger \tilde{\mathcal{O}}^{\alpha\beta} \Psi \rangle = -\hbar \text{tr} [\tilde{\mathcal{O}}^{\alpha\beta} G(x, x)], \quad (16)$$

where $\mathcal{O}^{\alpha\beta} = \eta_\alpha \sigma_\beta$, $\tilde{\mathcal{O}}^{\alpha\beta} = \eta_\alpha \sigma_\beta \tau_3$, and the trace is taken over the sublattice, valley, and spin indices.

Equation (14) admits, in general, many solutions. In order to select the solution which is the ground state of the system, we should calculate the energy density for each of these states, which is given by [36]

$$\mathcal{E} = \frac{i}{2} \int \frac{d\omega d^2p}{(2\pi)^3} \text{tr} \left[\left(-\omega - \mu_B \boldsymbol{\sigma} \mathbf{B} - m_0 \eta_3 \tau_3 + \frac{\hbar^2}{2m_*} \begin{pmatrix} 0 & D^- \\ D^+ & 0 \end{pmatrix} \right) \tilde{G}(\omega, \mathbf{p}) \right] - (\mu_{\alpha\beta} \rightarrow 0, \Delta_{\alpha\beta} \rightarrow 0), \quad (17)$$

where D^\pm are given by Eq. (B5) in Appendix B, and then determine the solution with the lowest energy density. For all phases (at $B_\perp = 0$), we use in what follows the full electron propagator in the Minkowski space,

$$\tilde{G}(\omega, \mathbf{k}) = \frac{1}{\omega + D_0 + \tilde{\Sigma} + i\epsilon \text{sgn} \omega}, \quad D_0 = \frac{\hbar^2}{2m_*} \begin{pmatrix} 0 & (k_x - ik_y)^2 \\ (k_x + ik_y)^2 & 0 \end{pmatrix}, \quad (18)$$

which we write in the form

$$\tilde{G}(\omega, \mathbf{k}) = \sum_j \frac{A_j(\mathbf{k})}{\omega - \tilde{E}_j(k) + i\epsilon \text{sgn} \omega}, \quad (19)$$

where $\tilde{E}_j(k)$ are the energy dispersions (the index j enumerates the branches of the spectrum) and $A_j(\mathbf{k})$ are matrices in the spin-valley-layer space.

Finally, since we consider bilayer graphene at the neutrality point, valid solutions should also satisfy the charge neutrality condition

$$n = i \int \frac{d\omega d^2k}{(2\pi)^3} \text{tr} [\tilde{G}(\omega, \mathbf{k})] = 0, \quad (20)$$

where trace runs over spin, valley, and sublattice indices. All our self-energy ansätze below satisfy the charge neutrality condition.

IV. SOLUTIONS IN THE ABSENCE OF MAGNETIC FIELD

In this section, we will solve the gap equations in electric field E_\perp in the case where external magnetic field is absent. In what follows, we set $\hbar = 1$.

A. The QAH, QSH, QVH, and LAF states in the absence of electric field

Let us discuss first the simplest case where the external electric field is absent and study the QAH, QSH, QVH, and LAF states. According to Eqs. (4), (15), and (16), the order parameter $\langle \Psi^\dagger \tau_3 \Psi \rangle$ of the QAH state is proportional to the Haldane mass Δ_{00} and describes a charge density wave with an opposite sign in the K and K' valleys, which is odd under time reversal. The order parameter $\langle \Psi^\dagger \sigma_j \tau_3 \Psi \rangle \sim \Delta_{0j}$ ($j = 1, 2, 3$) of the QSH state is antisymmetric in spin. The order parameter connected with the conventional Dirac mass $\langle \Psi^\dagger \eta_3 \tau_3 \Psi \rangle \sim \Delta_{30}$ is the order parameter of the QVH state and determines the charge-density imbalance between the two layers. The structure of this mass term coincides with that of the voltage imbalance term m_0 between the top and bottom gates introduced in Hamiltonian (2) and, therefore, can be considered as a dynamical counterpart of the latter. This mass term is even under time reversal. The Dirac mass term antisymmetric in spin $\langle \Psi^\dagger \sigma_j \tau_3 \Psi \rangle \sim \Delta_{3j}$ ($j = 1, 2, 3$) is the order parameter of the LAF state. Since the direction of the QSH and LAF state gaps in the spin space (subscript j in Δ_{0j} and Δ_{3j}) is completely arbitrary in the absence of an external magnetic field, we choose for the sake of convenience the third direction $j = 3$ in these gaps.

Let us derive the gap equations from the master gap equation (14) for the QAH, QSH, QVH, and LAF states. Since there are no external electric and magnetic fields, the first two terms on the right-hand side of Eq. (14) are absent. Substituting the corresponding ansatz for the self-energy into Eq. (14) allows us to establish the gap equations for each state in terms of their gaps. We find it convenient to use the notations Δ , Δ_z , m , and m_z for gaps Δ_{00} , Δ_{03} , Δ_{30} , and Δ_{33} , respectively. Thus, we use Δ and Δ_z to describe the QAH and QSH gaps with the Haldane-type masses and m and m_z to describe the QVH and LAF gaps with their Dirac-type gaps.

We assume that the dependence of gap functions on the energy is rather weak so that we can approximate these functions by their values at $\Omega = 0$ and neglect the dependence of V_{eff} on external energy, i.e., we approximate $V_{\text{eff}}(\Omega - \omega, \mathbf{p} - \mathbf{k}) \approx V_{\text{eff}}(\omega, \mathbf{p} - \mathbf{k})$. The momentum dependence of gaps generally results in the significant reduction in their sizes compared to the case of momentum-independent gaps.

The gap equations for the QAH ($\delta = \Delta$), QSH ($\delta = \Delta_z$), LAF ($\delta = m_z$) and QVH ($\delta = m$) phases have the form

$$\delta(p) = \delta_0 + \int \frac{d\omega d^2k}{(2\pi)^3} \frac{\delta(k)}{\omega^2 + E_k^2 + \delta^2(k)} \left[V_{\text{eff}}(\omega, \mathbf{p} - \mathbf{k}) + \frac{4\pi}{m_*} g_\delta \right], \quad (21)$$

where $E_k = k^2/(2m_*)$, the UV momentum integration cutoff $\sqrt{2m\Lambda}$ with $\Lambda = \gamma_1/4$ is used in our low-energy two-band model, the Wick's rotation $\omega \rightarrow i\omega$ has been made, and we used the following notations for the different linear combinations of the local interaction constants for the QAH, QSH, LAF, and QVH states:

$$g_\Delta = -2g_{z\perp} - 7g_{0z} + 2g_{\perp z} - 4g_{\perp\perp} + 2g_{\perp 0} + g_{z0} - 2g_{0\perp} + g_{zz}, \quad (22)$$

$$g_{\Delta_z} = -2g_{z\perp} + g_{0z} + 2g_{\perp z} - 4g_{\perp\perp} + 2g_{\perp 0} + g_{z0} - 2g_{0\perp} + g_{zz}, \quad (23)$$

$$g_{m_z} = -2g_{z\perp} + g_{0z} - 2g_{\perp z} + 4g_{\perp\perp} - 2g_{\perp 0} + g_{z0} - 2g_{0\perp} + g_{zz}, \quad (24)$$

$$g_m = -2g_{z\perp} + g_{0z} - 2g_{\perp z} + 4g_{\perp\perp} - 2g_{\perp 0} + g_{z0} - 2g_{0\perp} - 7g_{zz} + (m_*/\pi)V_{\text{IL}}(0). \quad (25)$$

The inhomogeneous term δ_0 in Eq. (21) is a bare gap, which is zero in the absence of external electric field. An analysis of the integral equations for momentum dependent gaps is presented in Appendix A. Typical solutions of gap equation (21) for $\delta_0 = 0$ and different values of coupling constants g_δ are presented in Fig. 1(a). The gaps monotonically decrease with momentum $|\mathbf{k}|$ approximately as $|\mathbf{k}|^{-1/2}$. In the approximation of momentum independent gaps, the integral equations are transformed into algebraic ones and we can compare the gap sizes of different states without actually solving the corresponding gap equations. Indeed, the solution of the gap equation (21) for a general gap parameter δ is a monotonously increasing function of g_δ , see Fig. 1(b) [the same is true for momentum-dependent $\delta(k)$]. Therefore, the ratio of the gap sizes in the different states is determined solely by the values of the effective local interaction constants g_m , g_{m_z} , g_{Δ_z} , and g_Δ . Note that for the QVH phase, the corresponding local interaction term g_m is effectively reduced because of the negative contribution $(m_*/\pi)V_{\text{IL}}(0) \equiv \tilde{v} \simeq -0.71/\kappa$.

One can see from Fig. 1(b) that, for small symmetry-breaking coupling constants $|g_{\alpha\beta}| \ll 1$, the gap magnitude in the absence of external fields is a few meV, which agrees well with the experimental values of the band gap 0.6–3 meV [11–14] (this corresponds to $-0.04 \lesssim g_\delta \lesssim 0.003$). The momentum dependence of gaps modifies the dispersion law for quasiparticle excitations, see Fig. 1(c), the energy of which now has a nontrivial minimum or maximum at nonzero $|\mathbf{k}|$.

In order to determine which of the broken symmetry states realizes the ground state of the system, their energy densities should be calculated by using Eq. (17). The energy densities for the states with δ denoting Δ_z , Δ , m , and m_z are given by

$$\mathcal{E}_0 = - \int \frac{d\omega d^2k}{2\pi^3} \left(\frac{2E_k^2 + \delta^2}{\omega^2 + E_k^2 + \delta^2} - \frac{2E_k^2}{\omega^2 + E_k^2} \right) = -C \frac{m_* \delta^2(0)}{2\pi}, \quad (26)$$

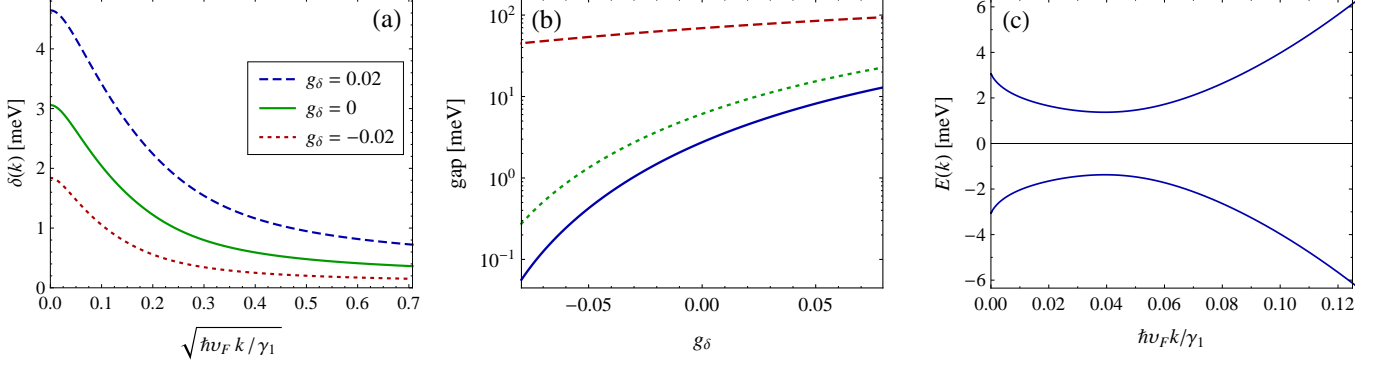


FIG. 1: (a) Solutions of gap equation (21) for $\delta_0 = 0$ and different values of g_δ . (b) The dependence of the band gap (solid line) and $2\delta(0)$ (dotted line) on the coupling constant g_δ shown on a logarithmic scale; the dashed line shows the band gap 2δ obtained within the approximation $\delta = \text{const}$. (c) The energy spectrum of the LAF state with $g_{m_z} = 0$. The value $\kappa = 1$ is used.

where the subscript in \mathcal{E}_0 refers to the fact that this is the energy density to the zeroth order in the perpendicular magnetic field. Further, $C = 1$ in the approximation $\delta(p) = \text{const}$, while the momentum dependence of $\delta(p)$ modifies it to $C \simeq 0.17 + 1.5g_\delta$. Equation (26) implies that the state with the largest gap has the lowest energy density and, therefore, is favored. Provided that $g_{\alpha\beta} \ll |\tilde{v}|$, the gap in the QVH state is smaller than gaps of the other states and, thus, the QVH phase is less energetically favorable. Further, we assume that the linear combination of the local interaction constants corresponding to the LAF phase is the largest one ($g_{m_z} > g_{\Delta_z}, g_\Delta$) so that the LAF phase is the most favorable one. This assumption [38] is based on the interpretation of the ground state in the strong magnetic field as the canted antiferromagnetic state [27, 37, 42] and the experimentally observed continuous evolution of this state when the magnetic field is reduced to zero [13].

B. Turning on electric field

When the electric field is turned on, gaps of various states have to mix in order to satisfy the gap equations. In particular, since the matrix structure of the term with m_0 in Eq.(2) generated by the external electric field in the gap equation is the same as the matrix structure of the gap of the QVH state, the order parameters of the QSH, QAH, and LAF states mix with the order parameter of the QVH state. The gap equations for these mixed QAH, QSH, and LAF states are

$$\begin{aligned} \delta(p) \pm m(p) &= \pm m_0 + \int \frac{d\omega d^2k}{(2\pi)^3} \frac{\delta(k) \pm m(k)}{\omega^2 + E_k^2 + [\delta(k) \pm m(k)]^2} \left[V_{\text{eff}}(\omega, \mathbf{p} - \mathbf{k}) + \frac{2\pi(g_\delta + g_m)}{m_*} \right] \\ &+ \int \frac{d\omega d^2k}{(2\pi)^3} \frac{\delta(k) \mp m(k)}{\omega^2 + E_k^2 + [\delta(k) \mp m(k)]^2} \frac{2\pi(g_\delta - g_m)}{m_*}, \quad \delta = \Delta, \Delta_z, m_z. \end{aligned} \quad (27)$$

In addition, the pure QVH state without any mixing still admits solutions even when the electric field is present. The gap equation for this state is given by

$$m(p) = m_0 + \int \frac{d\omega d^2k}{(2\pi)^3} \frac{m(k)}{\omega^2 + E_k^2 + m^2(k)} \left[V_{\text{eff}}(\omega, \mathbf{p} - \mathbf{k}) + \frac{4\pi}{m_*} g_m \right]. \quad (28)$$

Note that, as expected, Eq. (27) reduces to Eq. (21) with $\delta_0 = 0$ when m and m_0 are set to zero.

In order to determine the ground state, we should compare the energy densities of these states, which are determined by

$$\mathcal{E}_0 = -2\pi m_* \int \frac{d\omega}{2\pi} \int^\Lambda \frac{dE_k}{(2\pi)^2} \left[\frac{\Delta_+^2 + 2E_k^2 + m_0\Delta_+}{\omega^2 + \Delta_+^2 + E_k^2} + \frac{\Delta_-^2 + 2E_k^2 + m_0\Delta_-}{\omega^2 + \Delta_-^2 + E_k^2} - \frac{4E_k^2}{\omega^2 + E_k^2} \right], \quad (29)$$

where $\Delta_\pm = m \pm \Delta_z$ for the QSH state, $\Delta_\pm = m \pm \Delta$ for the QAH state, $\Delta_\pm = m \pm m_z$ for the LAF state, and finally $\Delta_\pm = m$ for the QVH state.

Since the gap equations (27) for different states differ only by the corresponding local interaction constants, one can easily see that, similarly to the case $E_{\perp} = 0$, the most favorable among the QSH, QAH, and LAF states is the state with the largest g_{δ} (which, according to our assumption, corresponds to the LAF state). On the other hand, a perpendicular electric field E_{\perp} is expected to favor the QVH state. When the electric field is weak, the term m_0 is only a perturbation to the gap equations (21). Therefore, the LAF state continues to have lower energy density than that of the QVH state for a certain range of m_0 . Whether the QVH state can eventually have lower energy density as m_0 varies to larger values depends on whether this state can lower its energy density faster than that of the LAF state.

We numerically solved the momentum-dependent gap equations for the LAF and QVH states and calculated their energy densities as functions of electric field E_{\perp} . The results are shown in Fig. 2 for $\kappa = 1$. At $E_{\perp} = 0$, our choice of the local four-fermion coupling constants ensures that the LAF state has the lowest energy density [see Fig. 2(a)] and, therefore, is the ground state. As the electric field becomes larger, the LAF solution ceases to exist and the pure QVH state becomes the ground state of the system at certain critical field E_{\perp}^{cr} which depends on the values of g_{m_z} and g_m . For the values of g_{m_z} and g_m in Fig. 2(c), the phase transition involves a jump discontinuity in the gaps [see Fig. 2(b)] and thus is the first-order one. The critical field at $g_{\alpha\beta} = 0$ ($g_{m_z} = 0$, $g_m = \tilde{v}$) is $E_{\perp}^{\text{cr}} \simeq 7.8$ mV/nm. If the value of g_{m_z} (which is the only parameter determining the size of the band gap at $E_{\perp} = 0$) is fixed, then the magnitude of the critical electric field is controlled solely by the coupling constant g_m . For example, if $g_{m_z} = 0$ (corresponding to the gap 2.7 meV), the experimental value $E_{\perp}^{\text{cr}} \simeq 15 - 20$ mV/nm [11, 13] implies $-1.1 \lesssim g_m - \tilde{v} \lesssim -0.66$.

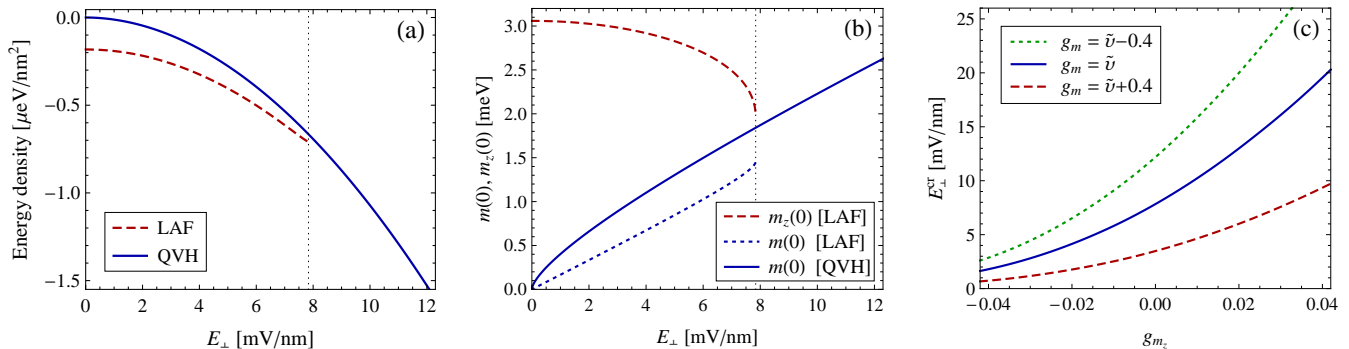


FIG. 2: The energy densities (a) and the gap parameters at $k = 0$ (b) of the LAF and QVH states in external electric field for $g_{m_z} = 0$, $g_m = \tilde{v}$. Panel (c) shows the dependence of the critical field E_{\perp}^{cr} for the LAF-QVH phase transition [vertical dotted line in panels (a) and (b)] on the local interaction constants g_{m_z} and g_m .

V. SOLUTIONS IN IN-PLANE MAGNETIC FIELD

In this section, we will study phases of the system in in-plane magnetic field and electric field perpendicular to the planes of graphene. Without the loss of generality, we can assume that the in-plane magnetic field is in the x direction $B_x \neq 0$; then the Zeeman interaction $Z\sigma_x$, $Z \equiv B_x\mu_B$, implies that the generalized chemical potential μ_x should be included in the analysis for all states.

A. Solutions in the absence of electric field

Let us analyze solutions of the gap equation first in the case where electric field is absent. The corresponding ansätze for the QVH, LAF, and QSH states can be written as follows:

$$\tilde{\Sigma}^{\text{QVH}} = -\mu_x\sigma_x - m\eta_3\tau_3, \quad (30)$$

$$\tilde{\Sigma}^{\text{QAH}} = -\mu_x\sigma_x - \Delta\tau_3, \quad (31)$$

$$\tilde{\Sigma}^{\text{LAF}} = -\mu_x\sigma_x - \mu_z\sigma_z - (m_x\sigma_x + m_z\sigma_z)\eta_3\tau_3, \quad (32)$$

$$\tilde{\Sigma}^{\text{QSH}} = -\mu_x\sigma_x - \mu_z\sigma_z - (\Delta_x\sigma_x + \Delta_z\sigma_z)\tau_3. \quad (33)$$

Note that the generalized chemical potentials and gaps of both x and z directions in spin space are present in the ansätze for the LAF and QSH states. In the absence of an in-plane magnetic field, the Zeeman term vanishes and the

direction of gaps in the spin space can be chosen arbitrarily. For $\mathbf{B}_{\parallel} \neq 0$, the directions along the magnetic field and perpendicular to it are physically different, therefore, both directions should be present in the most general ansätze for these states. For the QVH and QAH phases, the gap equations are

$$\mu_x(p) - Z = \frac{1}{2} \int \frac{d\omega d^2k}{(2\pi)^3} \left[V_{\text{eff}}(\omega, \mathbf{p} - \mathbf{k}) + \frac{4\pi}{m_*} g_{\mu} \right] \sum_{\lambda=\pm} \frac{\lambda \tilde{E}_{\lambda}(k)}{\omega^2 + \tilde{E}_{\lambda}^2(k)}, \quad (34)$$

$$\delta(p) = \frac{1}{2} \int \frac{d\omega d^2k}{(2\pi)^3} \left[V_{\text{eff}}(\omega, \mathbf{p} - \mathbf{k}) + \frac{4\pi}{m_*} g_{\delta} \right] \frac{\delta}{\sqrt{E_k^2 + \delta^2}} \sum_{\lambda=\pm} \frac{\tilde{E}_{\lambda}(k)}{\omega^2 + \tilde{E}_{\lambda}^2(k)}. \quad (35)$$

with

$$g_{\mu} = 2g_{z\perp} + g_{0z} + 2g_{\perp z} + 4g_{\perp\perp} + 2g_{\perp 0} + g_{z0} + 2g_{0\perp} + g_{zz}, \quad (36)$$

and the energy density given by

$$\mathcal{E}_0 = -2 \int \frac{d\omega d^2k}{(2\pi)^3} \left\{ \sum_{\lambda=\pm} \left[2E_k^2 + \delta^2 + \mu_x(Z + \mu_x) + \frac{\mu_x(3E_k^2 + 2\delta^2) + Z(E_k^2 + \delta^2)}{\lambda\sqrt{E_k^2 + \delta^2}} \right] \frac{1}{\omega^2 + \tilde{E}_{\lambda}^2(k)} - \frac{4E_k^2}{\omega^2 + E_k^2} \right\}, \quad (37)$$

where $\pm\tilde{E}_{\pm}(k)$ are four doubly degenerate branches of the energy dispersion, $\tilde{E}_{\pm}(k) \equiv \pm\mu_x + \sqrt{E_k^2 + \delta^2(k)}$, $\delta(p) = m(p)$ for the QVH phase and $\delta(p) = \Delta(p)$ for the QAH phase.

For the QSH and LAF state, one has the following set of gap equations ($\delta_x = \Delta_x$, $\delta_z = \Delta_z$ for the QSH phase and $\delta_x = m_x$, $\delta_z = m_z$ for the LAF phase)

$$\mu_x(p) - Z = \frac{1}{2} \int \frac{d\omega d^2k}{(2\pi)^3} \left[V_{\text{eff}}(\omega, \mathbf{p} - \mathbf{k}) + \frac{4\pi}{m_*} g_{\mu} \right] \sum_{\lambda=\pm} \frac{\mu_x + \lambda b^{-1} [E_k^2 \mu_x + \delta_x(\delta_x \mu_x + \delta_z \mu_z)]}{\omega^2 + \tilde{E}_{\lambda}^2(k)}, \quad (38)$$

$$\mu_z(p) = \frac{1}{2} \int \frac{d\omega d^2k}{(2\pi)^3} \left[V_{\text{eff}}(\omega, \mathbf{p} - \mathbf{k}) + \frac{4\pi}{m_*} g_{\mu} \right] \sum_{\lambda=\pm} \frac{\mu_z + \lambda b^{-1} [E_k^2 \mu_z + \delta_z(\delta_x \mu_x + \delta_z \mu_z)]}{\omega^2 + \tilde{E}_{\lambda}^2(k)}, \quad (39)$$

$$\delta_z(p) = \frac{1}{2} \int \frac{d\omega d^2k}{(2\pi)^3} \left[V_{\text{eff}}(\omega, \mathbf{p} - \mathbf{k}) + \frac{4\pi}{m_*} g_{\delta_z} \right] \sum_{\lambda=\pm} \frac{\delta_z + \lambda b^{-1} \mu_z (\delta_x \mu_x + \delta_z \mu_z)}{\omega^2 + \tilde{E}_{\lambda}^2(k)}, \quad (40)$$

$$\delta_x(p) = \frac{1}{2} \int \frac{d\omega d^2k}{(2\pi)^3} \left[V_{\text{eff}}(\omega, \mathbf{p} - \mathbf{k}) + \frac{4\pi}{m_*} g_{\delta_x} \right] \sum_{\lambda=\pm} \frac{\delta_x + \lambda b^{-1} \mu_x (\delta_x \mu_x + \delta_z \mu_z)}{\omega^2 + \tilde{E}_{\lambda}^2(k)}, \quad (41)$$

where

$$\tilde{E}_{\pm}(k) = \sqrt{E_k^2 + \delta_x^2 + \delta_z^2 + \mu_x^2 + \mu_z^2 \pm 2b}, \quad b = \sqrt{E_k^2(\mu_x^2 + \mu_z^2) + (\mu_x \delta_x + \mu_z \delta_z)^2}, \quad (42)$$

with the energy density

$$\mathcal{E}_0 = -2 \int \frac{d\omega d^2k}{(2\pi)^3} \left\{ \sum_{\lambda=\pm} \left[2E_k^2 + \delta_x^2 + \delta_z^2 + \mu_x(Z + \mu_x) + \mu_z^2 + \frac{E_k^2 [Z\mu_x + 3(\mu_x^2 + \mu_z^2)] + (\delta_x \mu_x + \delta_z \mu_z) [\delta_x(Z + 2\mu_x) + 2\delta_z \mu_z]}{\lambda b} \right] \frac{1}{\omega^2 + \tilde{E}_{\lambda}^2(k)} - \frac{4E_k^2}{\omega^2 + E_k^2} \right\}. \quad (43)$$

Clearly, the system of equations (38)–(41) immediately implies that $\mu_x \neq 0$ if $Z \neq 0$. Solutions of this system can be obtained only numerically. Our analysis shows that this system permits only gapped solutions with either δ_z or δ_x nonzero given by

$$\text{“noncollinear” solution:} \quad \mu_x \neq 0, \quad \delta_z \neq 0, \quad \mu_z = 0, \quad \delta_x = 0, \quad (44)$$

$$\text{“collinear” solution:} \quad \mu_x \neq 0, \quad \delta_x \neq 0, \quad \mu_z = 0, \quad \delta_z = 0, \quad (45)$$

and one gapless ferromagnetic solution with only μ_x different from zero. Solutions with both nonzero δ_z and δ_x are absent. The presence of nonzero μ_x (magnetization) in both solutions (44) and (45) means the admixture of the spin-polarized ferromagnetic order, see Eq. (16). The energy dispersion is given by four doubly degenerate eigenvalues

$\pm\tilde{E}_\pm(k)$, where $\tilde{E}_\pm(k) = \sqrt{(E_k \pm \mu_x)^2 + \delta_z^2}$ for noncollinear phases and $\tilde{E}_\pm(k) = \pm\mu_x + \sqrt{E_k^2 + \delta_z^2}$ for collinear ones. Evaluating the energy density, we find that the noncollinear solution has lower energy density than that of the collinear solution. The numerical calculations also reveal that, as in the absence of the magnetic field, our assumption $g_{m_z} > g_{\Delta_z}$ implies that the LAF solutions have lower energies than the QSH ones [see Fig. 3(a)]. Likewise, for $g_{m_z} > g_{\Delta_z}$, g_m the energy of the LAF solution is lower than that of the QAH and QVH ones, therefore, the noncollinear (canted) LAF phase remains the ground state for arbitrary B_\parallel . In this solution, the spin densities in the two layers have the opposite components in the yz plane, perpendicular to magnetic field and the equal components along the \mathbf{B} direction [19]. We also find that the energy density of the gapless ferromagnetic state is always higher than that of the noncollinear LAF and QSH states. In Fig. 3, we illustrate the magnetic field dependence of the free energies and the gaps of the collinear and noncollinear LAF and QSH phases. While the gapped noncollinear solutions exist at arbitrary magnetic fields, the spectrum gap in the collinear solutions closes at some finite B_\parallel value [Fig. 3(b)].

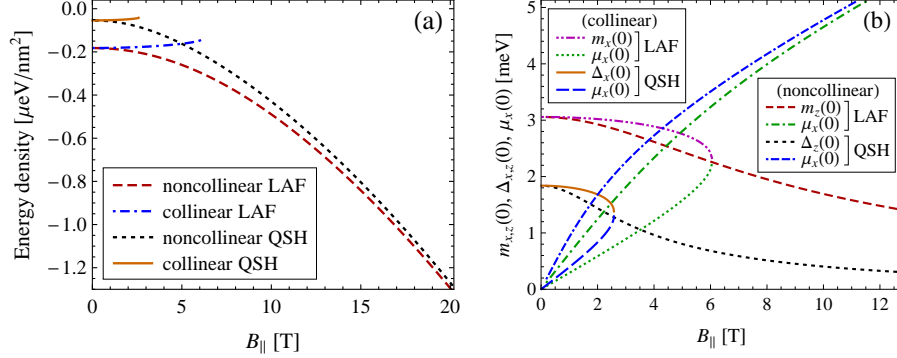


FIG. 3: The energy densities (a) and gaps at $k = 0$ (b) of the LAF and QSH states in external electric field for $g_{m_z} = 0$, $g_{\Delta_z} = -0.02$.

B. Turning on electric field

In this subsection, we study the phase diagram of the system in electric and in-plane magnetic fields. We find that it is determined by the competition between the QVH and LAF states. The corresponding ansätze for the QVH, QSH, and LAF states are given by

$$\tilde{\Sigma}^{\text{QVH}} = -\mu_x \sigma_x - m \eta_3 \tau_3, \quad (46)$$

$$\tilde{\Sigma}^{\text{QAH}} = -(\mu_x + \tilde{\mu}_x \eta_3) \sigma_x - (m \eta_3 + \Delta) \tau_3, \quad (47)$$

$$\tilde{\Sigma}^{\text{LAF}} = -\mu_x \sigma_x - (m \eta_3 + m_z \eta_3 \sigma_z) \tau_3, \quad (48)$$

$$\tilde{\Sigma}^{\text{QSH}} = -\mu_x \sigma_x - (m \eta_3 + \Delta_z \sigma_z) \tau_3. \quad (49)$$

In the above ansätze, we consider only the noncollinear LAF and QSH phases, assuming that they are more energetically favorable than their collinear counterparts, similarly to the case $E_\perp = 0$. Therefore, compared to Eqs. (30)–(33) we put $\mu_z = m_x = \Delta_x = 0$, and in addition all phases at $E_\perp \neq 0$ acquire an additional QVH gap component m (the ansatz for the QAH state should also include the generalized chemical potential $\tilde{\mu}_x$ for consistency).

The gap equations for the QVH state have the form

$$\mu_x(p) - Z = \frac{1}{2} \int \frac{d\omega d^2k}{(2\pi)^3} \left[V_{\text{eff}}(\omega, \mathbf{p} - \mathbf{k}) + \frac{4\pi}{m_*} g_\mu \right] \sum_{\lambda=\pm} \frac{\lambda \tilde{E}_\lambda(k)}{\omega^2 + \tilde{E}_\lambda^2(k)}, \quad (50)$$

$$m(p) - m_0 = \frac{1}{2} \int \frac{d\omega d^2k}{(2\pi)^3} \left[V_{\text{eff}}(\omega, \mathbf{p} - \mathbf{k}) + \frac{4\pi}{m_*} g_m \right] \frac{m}{\sqrt{E_k^2 + m^2}} \sum_{\lambda=\pm} \frac{\tilde{E}_\lambda(k)}{\omega^2 + \tilde{E}_\lambda^2(k)}, \quad (51)$$

with the corresponding energy density

$$\begin{aligned} \mathcal{E}_0 = & -2 \int \frac{d\omega d^2k}{(2\pi)^3} \left\{ \sum_{\lambda=\pm} \left[2E_k^2 + m(m_0 + m) + \mu_x(Z + \mu_x) \right. \right. \\ & \left. \left. + \frac{\mu_x(3E_k^2 + 2m^2 + mm_0) + Z(E_k^2 + m^2)}{\lambda\sqrt{E_k^2 + m^2}} \right] \frac{1}{\omega^2 + \tilde{E}_\lambda^2(k)} - \frac{4E_k^2}{\omega^2 + E_k^2} \right\}, \end{aligned} \quad (52)$$

where $\pm\tilde{E}_\pm(k)$, $\tilde{E}_\pm(k) \equiv \pm\mu_x + \sqrt{E_k^2 + m^2}$, are four doubly degenerate branches of the energy spectrum.

The gap equations for the QAH state read

$$\mu_\pm(p) - Z = \frac{1}{2} \int \frac{d\omega d^2k}{(2\pi)^3} \sum_{\lambda,\rho=\pm} \left[\frac{1 \pm \rho}{2} V_{\text{eff}}(\omega, \mathbf{p} - \mathbf{k}) + \frac{2\pi}{m_*} (g_\mu \pm \rho g_{\mu_z}) \right] \frac{\lambda \tilde{E}_{\lambda\rho}(k)}{\omega^2 + \tilde{E}_{\lambda\rho}^2(k)}, \quad (53)$$

$$\Delta_\pm(p) \mp m_0 = \frac{1}{2} \int \frac{d\omega d^2k}{(2\pi)^3} \sum_{\lambda,\rho=\pm} \left[\frac{1 \pm \rho}{2} V_{\text{eff}}(\omega, \mathbf{p} - \mathbf{k}) + \frac{2\pi}{m_*} (g_\Delta \pm \rho g_m) \right] \frac{\Delta_\rho}{\sqrt{E_k^2 + \Delta_\rho^2}} \frac{\tilde{E}_{\lambda\rho}(k)}{\omega^2 + \tilde{E}_{\lambda\rho}^2(k)}, \quad (54)$$

and the corresponding energy density is

$$\begin{aligned} \mathcal{E}_0 = & - \int \frac{d\omega d^2k}{(2\pi)^3} \left\{ \sum_{\lambda,\rho=\pm} \left[2E_k^2 + \Delta_\rho(\Delta_\rho + \rho m_0) + \mu_\rho(Z + \mu_\rho) \right. \right. \\ & \left. \left. + \frac{\mu_\rho(3E_k^2 + 2\Delta_\rho^2 + \rho m_0 \Delta_\rho) + Z(E_k^2 + \Delta_\rho^2)}{\lambda\sqrt{E_k^2 + \Delta_\rho^2}} \right] \frac{1}{\omega^2 + \tilde{E}_{\lambda\rho}^2(k)} - \frac{8E_k^2}{\omega^2 + E_k^2} \right\}, \end{aligned} \quad (55)$$

where $\pm\tilde{E}_{\pm\pm}(k)$ are eight energy eigenvalues, $\tilde{E}_{\pm,\rho}(k) = \pm\mu_\rho + \sqrt{E_k^2 + \Delta_\rho^2}$, $\Delta_\pm \equiv \Delta \pm m$, $\mu_\pm \equiv \mu_x \pm \tilde{\mu}_x$, and

$$g_{\tilde{\mu}_z} = 2g_{z\perp} + g_{0z} - 2g_{\perp z} - 4g_{\perp\perp} - 2g_{\perp 0} + g_{z0} + 2g_{0\perp} + g_{zz}. \quad (56)$$

For the LAF and QSH states, the gap equations are

$$\mu_x(p) - Z = \frac{1}{2} \int \frac{d\omega d^2k}{(2\pi)^3} \left[V_{\text{eff}}(\omega, \mathbf{p} - \mathbf{k}) + \frac{4\pi}{m_*} g_\mu \right] \sum_{\lambda=\pm} \left(1 + \frac{\lambda(E_k^2 + m^2)}{\sqrt{E_k^2 \mu_x^2 + m^2(\delta_z^2 + \mu_x^2)}} \right) \frac{\mu_x}{\omega^2 + \tilde{E}_\lambda^2(k)}, \quad (57)$$

$$m(p) - m_0 = \frac{1}{2} \int \frac{d\omega d^2k}{(2\pi)^3} \left[V_{\text{eff}}(\omega, \mathbf{p} - \mathbf{k}) + \frac{4\pi}{m_*} g_m \right] \sum_{\lambda=\pm} \left(1 + \frac{\lambda(\delta_z^2 + \mu_x^2)}{\sqrt{E_k^2 \mu_x^2 + m^2(\delta_z^2 + \mu_x^2)}} \right) \frac{m}{\omega^2 + \tilde{E}_\lambda^2(k)}, \quad (58)$$

$$\delta_z(p) = \frac{1}{2} \int \frac{d\omega d^2k}{(2\pi)^3} \left[V_{\text{eff}}(\omega, \mathbf{p} - \mathbf{k}) + \frac{4\pi}{m_*} g_{\delta_z} \right] \sum_{\lambda=\pm} \left(1 + \frac{\lambda m^2}{\sqrt{E_k^2 \mu_x^2 + m^2(\delta_z^2 + \mu_x^2)}} \right) \frac{\delta_z}{\omega^2 + \tilde{E}_\lambda^2(k)}, \quad (59)$$

where $\delta = m_z$ for the LAF state and $\delta = \Delta_z$ for the QSH state. Here $\pm\tilde{E}_\pm(k)$,

$$\tilde{E}_\pm(k) = \sqrt{E_k^2 + \delta_z^2 + m^2 + \mu_x^2 \pm 2\sqrt{E_k^2 \mu_x^2 + m^2(\delta_z^2 + \mu_x^2)}}, \quad (60)$$

are four doubly degenerate branches of the energy dispersion. The energy density is given by

$$\begin{aligned} \mathcal{E}_0 = & -2 \int \frac{d\omega d^2k}{(2\pi)^3} \left\{ \sum_{\lambda=\pm} \left[2E_k^2 + \delta_z^2 + m(m_0 + m) + \mu_x(Z + \mu_x) \right. \right. \\ & \left. \left. + \frac{\mu_x^2(3E_k^2 + 2m^2 + mm_0) + Z\mu_x(E_k^2 + m^2) + \delta_z^2 m(2m + m_0)}{\lambda\sqrt{E_k^2 \mu_x^2 + m^2(\delta_z^2 + \mu_x^2)}} \right] \frac{1}{\omega^2 + \tilde{E}_\lambda^2(k)} - \frac{4E_k^2}{\omega^2 + E_k^2} \right\}. \end{aligned} \quad (61)$$

Solutions of these gap equations can be obtained only numerically. In general, we found that all gaps weakly depend on B_{\parallel} and the main dependence on B_{\parallel} is contained in μ_x , see Fig. 4(c). The generalized chemical potential μ_x for the QSH and LAF states has an almost linear dependence on the magnetic field.

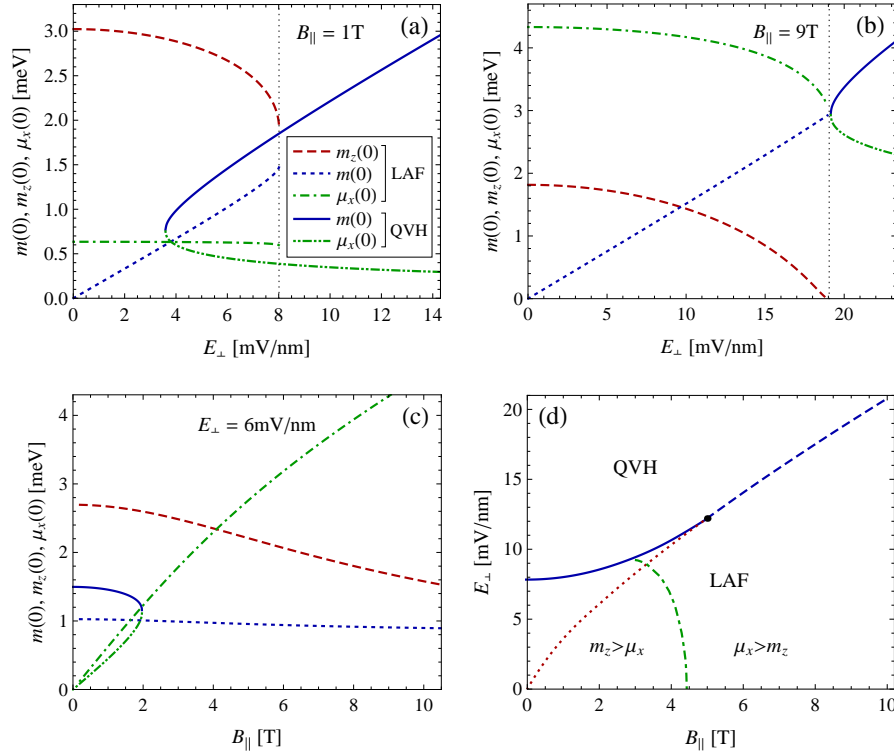


FIG. 4: The gaps at $k = 0$ of the LAF and QVH states as functions of external electric field for $B_{\parallel} = 1$ T (a) and $B_{\parallel} = 9$ T (b), of parallel magnetic field for $E_{\perp} = 6$ mV/nm (c) and the phase diagram in electric and in-plane magnetic fields (d). Parameters used: $g_{m_z} = g_{\mu} = 0$, $g_m = \bar{v}$, and $\kappa = 1$. The line types used in panels (a)–(c) are described in the inset of panel (a). In panel (d), the solid and dashed lines describe the first and second order phase transitions between the LAF and QVH states. The black point marks the critical point where the line of the first order phase transition terminates. The dotted line shows the boundary of the region of existence of the gapped QVH state and the dot-dashed line splits the LAF into regions where $m_z(k)$ or $\mu_x(k)$ dominates.

Having found the generalized chemical potentials and gaps, we can calculate and compare the energy densities of various states and then determine the phase diagram of the system. We find that the external electric and parallel magnetic fields do not change the ordering of the energies of the QAH, QSH, and LAF solutions and thus the ground state is not QAH or QSH. In Figs. 4(a) and 4(b) we plot the zero-momentum gaps for the LAF and QVH states as functions of an electric field for two values of the in-plane magnetic field, $B_{\parallel} = 1$ T and $B_{\parallel} = 9$ T, respectively. The largest gaps determine the system ground states. The corresponding phase diagram of bilayer graphene in electric and in-plane magnetic fields for the zero-momentum gaps is plotted in Fig. 4(c). The phase boundary, composed of the solid and dashed lines, separates the pure QVH and mixed LAF states. For the solid line part of the phase boundary ($B_{\parallel} \lesssim 5$ T), it is found that the phase transition is of the first order due to gaps changing discontinuously across the phase transition line while it is of the second order for the dashed line part ($B_{\parallel} \gtrsim 5$ T). The phase boundary for $B_{\parallel} \lesssim 5$ T is determined by a similar mechanism as in the case of zero B_{\parallel} . Again the mixed LAF phase exists only when external voltage is smaller than a certain critical value E_{\perp}^{cr} . As B_{\parallel} increases, the critical E_{\perp} increases also, while the energy density of the QVH state is not affected much by B_{\parallel} . The critical line is perfectly fitted by the quadratic dependence at small B_{\parallel}

$$E_{\perp}^{\text{cr}} = a + bB_{\parallel}^2, \quad (62)$$

where $a \simeq 7.8$ mV/nm and $b \simeq 0.18$ mV/(nm \times T 2) for $g_{\alpha\beta} = 0$ and $\kappa = 1$. On the other hand, if the value of g_{m_z} is determined from the experimental value of the band gap in the absence of external fields and g_m is determined from the experimental value of E_{\perp}^{cr} at $\mathbf{B} = 0$, then the phase diagram in Fig. 4 depends on a single free parameter g_{μ} . We found that although the values of a and b might change as g_{m_z} , g_m , and g_{μ} vary, the quadratic dependence of the critical line on the strength of in-plane magnetic field is preserved. For $B_{\parallel} \gtrsim 5$ T, the phase transition becomes a continuous one with the antiferromagnetic order parameter vanishing at the critical line. The latter has approximately linear dependence on B_{\parallel} .

We find that the noncollinear LAF phase is stable with respect to increasing the parallel magnetic field: although

for B_{\parallel} exceeding 3–5 T the Zeeman-like parameter $\mu_x(k)$ becomes larger than the antiferromagnetic gap $m_z(k)$ [see Figs. 4(c) and 4(d)], the latter does not vanish and this phase remains the ground state for all experimentally accessible magnetic fields. This behavior is in consonance with studies in monolayer [48] and bilayer [49] graphene where a transition from the easy-plane antiferromagnet to a pure ferromagnetic phase is not found. For earlier studies of the role of in-plane magnetic field in specific (2 + 1)-dimensional Gross-Neveu model, see Ref. [50]. Experimentally, the gapped ground state in suspended bilayer was found to be stable in parallel magnetic fields at least up to 3 T in Ref. [43].

The critical line in Fig. 4 qualitatively agrees with the findings in Ref. [42], where the phase diagram of the $\nu = 0$ state in bilayer graphene was experimentally studied as a function of perpendicular electric and total magnetic B_{tot} fields with the out-of-plane magnetic field fixed at $B_{\perp} = 1.75$ T. Experimentally, at low B_{tot} , the phase boundary between the QVH and CAF phases is practically flat. The CAF state at $B_{\perp} \neq 0$ continuously interpolates between the LAF and ferromagnetic states as the in-plane magnetic field increases [27, 37], and at small B_{\perp} it is not much different from the (noncollinear) LAF state considered in our analysis. For B_{tot} larger than approximately 15 T, the critical electric field separating the QVH and ferromagnetic phases increases with B_{tot} linearly [42]. In our analysis, the critical line between the QVH and LAF states for $B_{\parallel} \gtrsim 5$ T also has a linear shape with approximately the same slope of 1.7 mV/(nm×T). Thus, the phase diagram obtained in Ref. [42] (see Fig. 4 therein) has many similar features to our phase diagram at $B_{\perp} = 0$. The main difference from Ref. [42] is that according to our phase diagram the canted LAF state remains a stable ground state in the absence of out-of-plane magnetic field at large B_{\parallel} : There is no phase transition to a ferromagnetic state with conductance $4e^2/h$ due to topologically protected edge states. Since the LAF state does not have edge states, the absence of a phase transition at $B_{\perp} = 0$ can be checked experimentally.

VI. LINEAR AND QUADRATIC IN B_{\perp} CORRECTIONS

In this section, we focus our analysis on the gap generation in a weak perpendicular magnetic field and set, for simplicity, $B_{\parallel} = 0$. We treat B_{\perp} as a perturbation and consider the corrections to the generalized chemical potentials, gaps, and energy densities in the linear and quadratic orders in B_{\perp} . The corresponding results for the fermion propagator are given in Appendix B. This perturbative analysis is expected to be valid when the cyclotron energy $\hbar\omega_c = e\hbar B_{\perp}/(m_*c) \approx 2.2B_{\perp}[\text{T}]$ meV is much less than the dynamically generated gap at $B_{\perp} = 0$. Taking into account the experimentally observed band gaps up to 3 meV [11–14], we have the condition $B_{\perp} \ll 1$ T. In order to simplify our analysis, we will not consider in-plane magnetic field in this section. Moreover, due to the complexity of the gap equation, we will consider only momentum-independent generalized chemical potentials and gaps. Since this approximation leads to the systematic overestimation of both the gap magnitudes and E_{\perp}^{cr} , we use $\kappa = 3$ in order to keep them closer to the experimental values.

In order to use Eq. (14) and obtain a self-consistent and recursive system of equations, we should first specify the ansatz for the QVH and LAF states. Due to the Zeeman term, we should include $\mu_{03} \equiv \mu_z \neq 0$ in ansatz (15) for both the QVH and LAF states in order that the gap equations have consistent solutions. Therefore, the full ansatz for these two states is given by

$$\text{QVH: } \tilde{\Sigma} = -m\eta_3\tau_3 - B_{\perp}(\mu_z^{(1)}\sigma_3 + \tilde{\mu}^{(1)}\eta_3) - B_{\perp}^2(m^{(2)}\eta_3\tau_3 + \Delta_z^{(2)}\sigma_3\tau_3), \quad (63)$$

$$\begin{aligned} \text{LAF: } \tilde{\Sigma} = & -m_x\sigma_1\eta_3\tau_3 - m\eta_3\tau_3 - B_{\perp}(\mu_z^{(1)}\sigma_3 + \tilde{\mu}_x^{(1)}\sigma_1\eta_3 + \tilde{\mu}^{(1)}\eta_3) \\ & - B_{\perp}^2(m_x^{(2)}\sigma_1\eta_3\tau_3 + m^{(2)}\eta_3\tau_3 + \Delta_z^{(2)}\sigma_3\tau_3). \end{aligned} \quad (64)$$

Note that the $\mathcal{O}(B_{\perp}^0)$ antiferromagnetic gap parameter m_x is perpendicular to the external magnetic field (in general, it points in an arbitrary direction in the graphene sheet plane), while the $\mathcal{O}(B_{\perp}^1)$ parameter $\mu_z^{(1)}$ leads to a small tilting in the \mathbf{B} direction. Similarly to the previously considered case of a parallel magnetic field, our numerical calculations show that this noncollinear orientation lowers the energy of the system and is thus favorable. Hence, the perpendicular magnetic field transforms the purely antiferromagnetic state into the canted antiferromagnetic one [27, 37], therefore, in what follows we will use the notation CAF for this state. The corresponding gap equations in the quadratic order in B_{\perp} for the parameters entering ansätze (63), (64) can be obtained from Eq. (14) and are written down in Appendix B.

Solving the gap equations numerically and then substituting the solutions in the energy density (B22), we found that the first order in B_{\perp} correction to the energy density is zero for both the QVH and CAF states and a nonzero contribution is connected with the second order in B_{\perp} correction as shown in Fig. 5(b). It is seen that this correction is positive for the the QVH phase and negative for the LAF phase. Therefore, the point where the energies cross at $\mathbf{B} = 0$ [see Fig. 5(a)] shifts towards the larger E_{\perp} values with growing B_{\perp} while remaining the first order transition. The resulting critical line has the form $E_{\perp}^{\text{cr}} = a + bB_{\perp}^2$ and is plotted in Fig. 5(c). Experimentally, the existence of this phase transition has been proven but the exact expression for this critical line is still not clear.

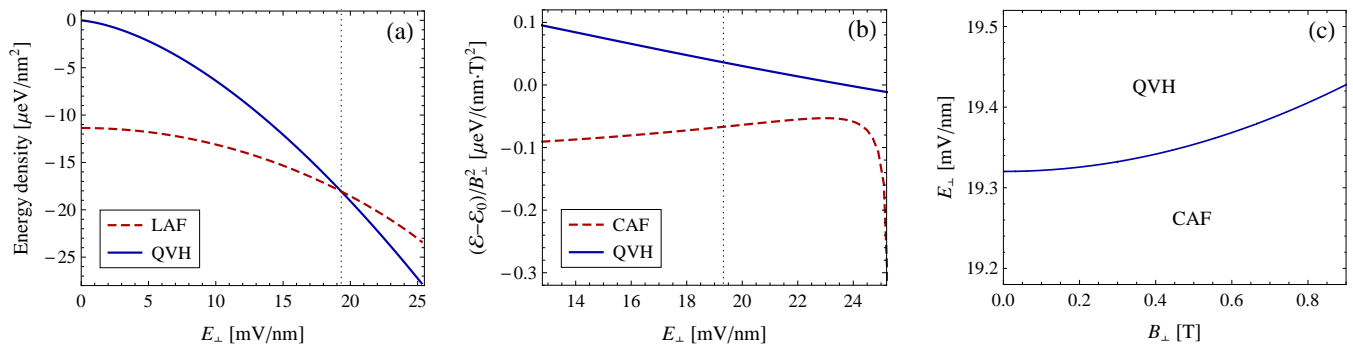


FIG. 5: The energy densities of the LAF and QVH states at $\mathbf{B} = 0$ (a), their corrections due to finite B_{\perp} in the vicinity of the phase transition at $E_{\perp} = E_{\perp}^{\text{cr}}$ (marked by the vertical dotted line) (b), and the phase diagram in the (B_{\perp}, E_{\perp}) plane (c) for $g_{\alpha\beta} = 0$ and $\kappa = 3$.

VII. CONCLUSION

In this paper, we studied the gap generation and dynamical SU(4) symmetry breaking in bilayer graphene at the neutrality point in electric and in-plane magnetic fields as well as a weak out-of-plane magnetic field \mathbf{B}_{\perp} . We utilize a model with the dynamically screened Coulomb interaction and contact four-fermion interactions which explicitly break the SU(4) valley-spin symmetry. We emphasize the following new points in our analysis. Although it was found [27, 37, 38] that the contact four-fermion interactions are crucial for the correct choice of the ground state of bilayer graphene, a study of broken symmetry states in a model with both the long-range Coulomb interaction and SU(4) asymmetric contact interactions was never done in the literature. Further, beginning with the pioneer work [8], the approximation of momentum-independent gaps was applied in all studies of the gap equations. This is indeed a reasonable first approximation because the polarization effects in bilayer graphene are much stronger than those in monolayer graphene and the static screened Coulomb potential in bilayer graphene is approximately constant in a large interval of momenta. However, it is very important to take into account the frequency dependence of polarization effects which significantly decrease screening. In this case, our study shows that the momentum dependence of gaps, which can be approximated by $|\mathbf{k}|^{-1/2}$ at large momenta, is essential and diminishes by an order of magnitude the gaps compared to the case of the momentum-independent approximation.

By numerically solving the momentum-dependent gap equations for the broken symmetry states and determining their energy densities as functions of electric field E_{\perp} and in-plane magnetic field B_{\parallel} , we found that the LAF phase is realized at small values of E_{\perp} , while the QVH phase is the ground state of the system at large E_{\perp} . As in-plane magnetic field B_{\parallel} increases, the critical electric field E_{\perp}^{cr} increases too. The part of the critical line separating the LAF and QVH phases at magnetic field $B_{\parallel} \lesssim 5\text{T}$ has a quadratic dependence $E_{\perp}^{\text{cr}} = a + bB_{\parallel}^2$, and we found that the phase transition across this line is of the first order due to gaps changing discontinuously. For $B_{\parallel} \gtrsim 5\text{T}$, the critical line has approximately linear dependence on B_{\parallel} and the phase transition becomes a continuous one.

We show that although the SU(4)-asymmetric contact interactions include, in general, eight independent constants, the gap sizes and energy density of the ground LAF state, experimentally observed in the absence of external fields, are controlled by a single linear combination g_{m_z} . Furthermore, in order to describe other broken symmetry ground states in perpendicular electric and in-plane magnetic fields, one should take into account two additional linear combinations g_m and g_{μ} . Thus the phase diagram in the $(B_{\parallel}, E_{\perp})$ plane is parametrized by the three independent effective local interaction constants. We found that for some reasonable choice of these parameters the band gap and the critical electric field at $\mathbf{B} = 0$ agree well with the corresponding experimental data available in the literature. According to our phase diagram, the (canted) LAF state remains a stable ground state in the absence of out-of-plane magnetic field at large B_{\parallel} : There is no phase transition at low displacement field E_{\perp} . This result is similar to studies in monolayer [48] and bilayer [49] graphene where a transition from the antiferromagnetic to a pure ferromagnetic phase was not found. Since the LAF state does not have edge states, the absence of a phase transition at $B_{\perp} = 0$ driven by in-plane magnetic field can be checked experimentally. Given that existing experiments at $B_{\perp} \geq 1.75\text{T}$ [42, 51] support the scenario of the CAF to ferromagnetic state phase transition in the strong parallel fields [27], it would be interesting to investigate theoretically the fate of this transition in the $(B_{\perp}, B_{\parallel})$ plane at smaller B_{\perp} values. This question will be addressed elsewhere.

We studied the role of weak perpendicular magnetic field in the particular case of zero in-plane magnetic field. By using a perturbation theory in a perpendicular magnetic field $B_{\perp} \ll 1\text{T}$ with $B_{\parallel} = 0$, we found that the broken symmetry states and phase diagram are stable and remain qualitatively unchanged. The main consequence of the

presence of B_\perp is that the LAF state transforms into the CAF state in agreement with previous theoretical and experimental studies.

Finally, we would like to add that studied broken states may find practical applications. For instance, recently it was proposed [52] that the CAF state could be instrumental for the creation of topological superconductivity in graphene-superconductor junctions without the need for strong spin-orbit coupling. The key advantage of the CAF state is its magnetic ordering due to the contact four-fermion interactions. Therefore, coupling this state to a conventional superconductor gives rise to Majorana bound states and makes the CAF state a promising platform for Majorana physics in graphene systems.

Acknowledgments

We thank V.A. Miransky for fruitful discussions. The work of Junji Jia is supported by the Chinese SRFDP 20130141120079, NNSF China 11504276 & 11547310, Ministry of Science and Technology of China (Grant No. 2014GB109004), and Natural Science Foundation of Hubei Province (Grant No. ZRY2014000988). V.P.G. acknowledges the support of the RISE Project CoExAN GA644076. The work of E.V.G and V.P.G. was supported partially by the Program of Fundamental Research of the Physics and Astronomy Division of the NAS of Ukraine.

Appendix A: Momentum-dependent gap parameters

In this section we solve the gap equations keeping the momentum dependence of the gap parameters (the frequency dependence is neglected). Let us start with the gap equation

$$\delta(p) = \delta_0 + \int \frac{d\omega d^2k}{(2\pi)^3} \frac{\delta(k)}{\omega^2 + E_k^2 + \delta^2(k)} \left[V_{\text{eff}}(\omega, \mathbf{p} - \mathbf{k}) + \frac{4\pi}{m_*} g_\delta \right] \quad (\text{A1})$$

for a general gap parameter $\delta(p)$, where δ_0 is a bare gap and g_δ is the corresponding local interaction constant. Using Eqs. (10) and (11), the above equation can be written as

$$\delta(p) = \delta_0 + \frac{1}{4\pi^2} \int_0^\infty d\omega \int_0^{2\pi} d\theta_k \int_0^\Lambda dE_k \frac{\delta(k)}{\omega^2 + E_k^2 + \delta^2(k)} \left(\frac{1}{\alpha^{-1} \sqrt{E_{\mathbf{p}-\mathbf{k}}/\gamma_1} + 2P(\omega/E_{\mathbf{p}-\mathbf{k}})} + 4g_\delta \right), \quad (\text{A2})$$

where θ_k is the angle between vectors \mathbf{k} and \mathbf{p} , and $\alpha = e^2/(\kappa v_F) \simeq 2.7/\kappa$ is the graphene's effective "fine structure constant". The frequency integration can be done for the approximate form of the polarization function [8]

$$P(z) \approx \frac{1}{2} \left(\frac{z^2}{\pi^2} + \frac{1}{4 \ln^2 4} \right)^{-1/2}, \quad (\text{A3})$$

which respects the asymptotics $P(0) = \ln 4$, $P(z \gg 1) \simeq \pi/(2z)$ of the original polarization function (11). Using expression (A3) for the polarization function and the formula

$$\int_0^\infty \frac{dx}{(x^2 + 1)(u + 1/\sqrt{1 + v^2 x^2})} = \frac{1}{u^2(v^2 - 1) + 1} \left[\frac{v \arctan \sqrt{u^2 - 1}}{\sqrt{u^2 - 1}} + \frac{\pi}{2} u(v^2 - 1) + \sqrt{1 - v^2} \arctan \frac{\sqrt{1 - v^2}}{v} \right] \quad (\text{A4})$$

$$\equiv F(u, v), \quad (\text{A5})$$

one gets from Eq. (A2)

$$\delta(p) = \delta_0 + \frac{1}{2\pi} \int_0^{2\pi} d\theta_k \int_0^\Lambda dE_k \left[K(|\mathbf{p} - \mathbf{k}|, \sqrt{E_k^2 + \delta^2(k)}) + g_\delta \right] \frac{\delta(k)}{\sqrt{E_k^2 + \delta^2(k)}}, \quad (\text{A6})$$

where

$$K(q, f(k)) = \frac{1}{4\pi \ln 4} F \left(\frac{\sqrt{E_q/\gamma_1}}{2\alpha \ln 4}, \frac{2 \ln 4}{\pi E_q} f(k) \right). \quad (\text{A7})$$

The angular integration can be performed if one uses the following approximation for the kernel:

$$K(|\mathbf{p} - \mathbf{k}|, f(k)) \approx K(\max(p, k), f(k)) \equiv \tilde{K}(p, k, f(k)), \quad (\text{A8})$$

and we finally arrive at

$$\delta(p) = \delta_0 + \int_0^\Lambda dE_k \left[\tilde{K}\left(p, k, \sqrt{E_k^2 + \delta^2(k)}\right) + g_\delta \right] \frac{\delta(k)}{\sqrt{E_k^2 + \delta^2(k)}}. \quad (\text{A9})$$

The above gap equation can be used for the LAF, QSH, QAH, and QVH states in the simplest cases; for example, with $\delta(p) = m(p)$, $\delta_0 = m_0$ it coincides with Eq. (28) for the QVH state at $\mathbf{B} = 0$. The generalization to the case of a system of a few gap equations is also straightforward. We solve the resulting integral equations of the form (A9) iteratively by using a discrete momentum grid k_i with a few hundred points, uniform in $k^{1/4}$. Starting from some initial guess for $\delta(k_i)$, we then either evaluate the right-hand side directly (with the integral calculated by the trapezoidal rule) or solve the resulting system of linear equations for $\delta(k_i)$ [$\delta(k_i)$ in the denominator of the integrand and in the kernel \tilde{K} are taken from the previous iteration step], whichever leads to the convergent iterations.

Figure 1(a) shows the momentum-dependent gap $m_z(p)$ in the LAF state with $g_{m_z} = 0$ in the absence of external fields, obtained by numerically solving Eq. (A9) with $g_\delta = 0$, $\delta_0 = 0$. The energy spectrum has the ‘‘mexican-hat’’ form, see Fig. 1(c).

Appendix B: Gap equations in the second order in B_\perp

As mentioned in the Introduction, our aim is to study the gap generation in bilayer graphene in perturbation theory in perpendicular magnetic field with $B_\parallel = 0$. By making use of Eq. (12), let us express the fermion propagator through the self-energy in the perturbation theory in B_\perp . The free inverse fermion propagator in an external magnetic field is given by

$$S^{-1}(x, z) = \left(i\hbar\partial_{x_0} + \frac{\hbar^2}{2m_*} \begin{pmatrix} 0 & (-iD_{x_1} - D_{x_2})^2 \\ (-iD_{x_1} + D_{x_2})^2 & 0 \end{pmatrix} \right) \delta^3(x - z) \quad (\text{B1})$$

with the covariant derivative $D_k = \partial_k + (ie/\hbar c)A_k$ ($e > 0$). Further, by writing

$$\int d^3z S^{-1}(x, z)G(z, y) = e^{i\Phi(x, y)} \left(i\hbar\partial_{x_0 - y_0} + \frac{\hbar^2}{2m_*} \begin{bmatrix} 0 & (-iD_{x_1 - y_1} - D_{x_2 - y_2})^2 \\ (-iD_{x_1 - y_1} + D_{x_2 - y_2})^2 & 0 \end{bmatrix} \right) \tilde{G}(x - y), \quad (\text{B2})$$

and using the identity

$$\mathbf{x}\mathbf{A}(\mathbf{z}) + \mathbf{z}\mathbf{A}(\mathbf{y}) = \mathbf{x}\mathbf{A}(\mathbf{y}) + (\mathbf{x} - \mathbf{y})\mathbf{A}(\mathbf{z} - \mathbf{y}), \quad (\text{B3})$$

for the quantity $\mathbf{x}\mathbf{A}(\mathbf{y}) = -(B_\perp/2)(\mathbf{x} \times \mathbf{y}) \equiv -(B_\perp/2)\epsilon_{ij}x_i y_j$, $i, j = 1, 2$, Eq. (12) in momentum space takes the form

$$\left(\omega + \frac{\hbar^2}{2m_*} \begin{pmatrix} 0 & D^- \\ D^+ & 0 \end{pmatrix} \right) \tilde{G}(\omega, \mathbf{p}) + \int d^2(\mathbf{x} - \mathbf{y}) e^{-i\mathbf{p}(\mathbf{x} - \mathbf{y})} \int d^2\mathbf{z} e^{-i(e/\hbar c)(\mathbf{x} - \mathbf{y})\mathbf{A}(\mathbf{z} - \mathbf{y})} \tilde{\Sigma}(\omega, \mathbf{x} - \mathbf{z}) \tilde{G}(\omega, \mathbf{z} - \mathbf{y}) = 1, \quad (\text{B4})$$

where

$$D^\mp = (p_1 \mp ip_2)^2 \pm \frac{eB_\perp}{\hbar c} (p_1 \mp ip_2)(\partial_{p_1} \mp i\partial_{p_2}) + \frac{e^2 B_\perp^2 (\partial_{p_1} \mp i\partial_{p_2})^2}{4(\hbar c)^2}. \quad (\text{B5})$$

In what follows for simplicity we put $\hbar = c = 1$. Equations (14) and (B4) form a system of two equations for the translation invariant functions $\tilde{\Sigma}$ and \tilde{G} .

Perpendicular magnetic field B_\perp enters these equations only through Eq. (B4). Since we seek the generalized chemical potentials and gaps up to the second order in B_\perp , we expand Eq. (B4) up to B_\perp^2 terms. In fact, we have to expand only the factor $\exp[-ie(\mathbf{x} - \mathbf{y})\mathbf{A}(\mathbf{z} - \mathbf{y})]$ because D^+ and D^- given by Eq. (B5) are quadratic polynomials in B_\perp . Expanding the last term in Eq. (B4) up to the second order in B_\perp , we find

$$\begin{aligned} & \int d^2(\mathbf{x} - \mathbf{y}) e^{-i\mathbf{p}(\mathbf{x} - \mathbf{y})} \int d^2\mathbf{z} e^{-ie(\mathbf{x} - \mathbf{y})\mathbf{A}(\mathbf{z} - \mathbf{y})} \tilde{\Sigma}(\omega, \mathbf{x} - \mathbf{z}) \tilde{G}(\omega, \mathbf{z} - \mathbf{y}) \\ & \approx \left(1 - \frac{ieB_\perp}{2} \frac{\partial_{\mathbf{p}} \times \partial_{\mathbf{k}}}{2} - \frac{e^2 B_\perp^2}{8} (\partial_{\mathbf{p}} \times \partial_{\mathbf{k}})^2 \right) \tilde{\Sigma}(\omega, \mathbf{p}) \tilde{G}(\omega, \mathbf{k})|_{\mathbf{k}=\mathbf{p}}. \end{aligned} \quad (\text{B6})$$

Actually, it is possible to calculate this term in momentum space exactly and it is given by the star product [53] of the translation invariant self-energy and propagator

$$\int d^2(\mathbf{x} - \mathbf{y}) e^{-i\mathbf{p}(\mathbf{x} - \mathbf{y})} \int d^2\mathbf{z} e^{-ie(\mathbf{x} - \mathbf{y})\mathbf{A}(\mathbf{z} - \mathbf{y})} \tilde{\Sigma}(\omega, \mathbf{x} - \mathbf{z}) \tilde{G}(\omega, \mathbf{z} - \mathbf{y}) = e^{-ieB_\perp \partial_{\mathbf{p}} \times \partial_{\mathbf{k}}/2} \tilde{\Sigma}(\omega, \mathbf{p}) \tilde{G}(\omega, \mathbf{k})|_{\mathbf{k}=\mathbf{p}}. \quad (\text{B7})$$

Thus, Eq. (B4) in the second order in B_\perp takes the form

$$\left(\omega + \frac{\hbar^2}{2m_*} \begin{pmatrix} 0 & D^- \\ D^+ & 0 \end{pmatrix} \right) \tilde{G}(\omega, \mathbf{p}) + \left(1 - \frac{ieB_\perp \partial_{\mathbf{p}} \times \partial_{\mathbf{k}}}{2} - \frac{e^2 B_\perp^2}{8} (\partial_{\mathbf{p}} \times \partial_{\mathbf{k}})^2 \right) \tilde{\Sigma}(\omega, \mathbf{p}) \tilde{G}(\omega, \mathbf{k})|_{\mathbf{k}=\mathbf{p}} = 1. \quad (\text{B8})$$

Equations (14) and (B8) define the translation invariant self-energy and propagator up to the second order in B_\perp . These equations are the starting point for the subsequent analysis in Sec. VI. We first rewrite Eq. (B8) as follows:

$$(\omega + D_0 + B_\perp D_1 + B_\perp^2 D_2)(\tilde{G}_0 + B_\perp \tilde{G}_1 + B_\perp^2 \tilde{G}_2) + (\tilde{\Sigma}_0 + B_\perp \tilde{\Sigma}_1 + B_\perp^2 \tilde{\Sigma}_2)(\tilde{G}_0 + B_\perp \tilde{G}_1 + B_\perp^2 \tilde{G}_2) = 1, \quad (\text{B9})$$

where D_i and $\tilde{\Sigma}_i$ can be read off from Eqs. (B5) and (15). \tilde{G}_i ($i = 0, 1, 2$) represent the full propagators to various orders in B_\perp . By making use of Eq. (B9), we find

$$\tilde{G}_0 = \frac{1}{\omega + D_0 + \tilde{\Sigma}_0}, \quad (\text{B10})$$

$$\tilde{G}_1 = -\frac{1}{\omega + D_0 + \tilde{\Sigma}_0} (D_1 + \tilde{\Sigma}_1) \tilde{G}_0, \quad (\text{B11})$$

$$\tilde{G}_2 = -\frac{1}{\omega + D_0 + \tilde{\Sigma}_0} \left[(D_1 + \tilde{\Sigma}_1) \tilde{G}_1 + (D_2 + \tilde{\Sigma}_2) \tilde{G}_0 \right]. \quad (\text{B12})$$

Using the obtained expressions for the coefficients of the fermion propagator in expansion in B_\perp , we write down the gap equations for the studied states.

For the QVH state, we have in the first order in B_\perp

$$\mu_z^{(1)} - \mu_B = \int \frac{d\omega d^2k}{(2\pi)^3} \frac{\mu_z^{(1)} (\omega^2 - E_k^2 - m^2)}{(\omega^2 + E_k^2 + m^2)^2} \left[V_{\text{eff}}(\omega, \mathbf{k}) + \frac{4\pi}{m_*} g_\mu \right], \quad (\text{B13})$$

$$\tilde{\mu}^{(1)} = \int \frac{d\omega d^2k}{(2\pi)^3} \frac{\tilde{\mu}^{(1)} (\omega^2 - E_k^2 - m^2) - 4\chi m E_k}{(\omega^2 + E_k^2 + m^2)^2} \left[V_{\text{eff}}(\omega, \mathbf{k}) + \frac{4\pi}{m_*} g_{\tilde{\mu}} \right], \quad (\text{B14})$$

where $\chi = e/(2m_*c)$ and

$$g_{\tilde{\mu}} = 2g_{z\perp} + g_{0z} - 2g_{\perp z} - 4g_{\perp\perp} - 2g_{\perp 0} - 7g_{z0} + 2g_{0\perp} + g_{zz}. \quad (\text{B15})$$

In the order B_\perp^2 , we have

$$m^{(2)} = \int \frac{d\omega d^2k}{(2\pi)^3} \left[\frac{2\chi^2 m [9E_k^4 - (\omega^2 + m^2)^2]}{(\omega^2 + E_k^2 + m^2)^4} + \frac{m^{(2)} (E_k^2 + \omega^2 - m^2)}{(\omega^2 + E_k^2 + m^2)^2} \right. \\ \left. + \frac{(E_k^2 + m^2 - 3\omega^2) \{ m [(\mu_z^{(1)})^2 + (\tilde{\mu}^{(1)})^2] + 4\chi \tilde{\mu}^{(1)} E_k \}}{(\omega^2 + E_k^2 + m^2)^3} \right] \left[V_{\text{eff}}(\omega, \mathbf{k}) + \frac{4\pi}{m_*} g_m \right], \quad (\text{B16})$$

$$\Delta_z^{(2)} = \int \frac{d\omega d^2k}{(2\pi)^3} \left[\frac{\Delta_z^{(2)} (E_k^2 + \omega^2 - m^2)}{(\omega^2 + E_k^2 + m^2)^2} + \frac{2\mu_z^{(1)} (m\tilde{\mu}^{(1)} + 2\chi E_k) (E_k^2 + m^2 - 3\omega^2)}{(\omega^2 + E_k^2 + m^2)^3} \right] \left[V_{\text{eff}}(\omega, \mathbf{k}) + \frac{4\pi}{m_*} g_{\Delta_z} \right] \quad (\text{B17})$$

[for the gap equation in the zeroth order in B_\perp , see Eq. (28)]. For the LAF state, the zeroth order in B_\perp gap equation is given by Eq. (27) with $\delta = m_x$, the $\mathcal{O}(B_\perp)$ gap equation reads

$$\mu_z^{(1)} - \mu_B = -\frac{\mu_z^{(1)}}{2} \int \frac{d\omega d^2k}{(2\pi)^3} \sum_{\lambda=\pm} \left(1 + \frac{\lambda(\omega^2 + m_x^2)}{mm_x} \right) \frac{1}{\omega^2 + E_k^2 + m_\lambda^2} \left[V_{\text{eff}}(\omega, \mathbf{k}) + \frac{4\pi}{m_*} g_\mu \right], \quad (\text{B18})$$

$$\tilde{\mu}_\pm = \int \frac{d\omega d^2k}{(2\pi)^3} \sum_{\lambda=\pm} \left[\frac{1 \pm \lambda}{2} V_{\text{eff}}(\omega, k) + \frac{2\pi}{m_*} (g_{\tilde{\mu}} \pm \lambda g_{\tilde{\mu}_z}) \right] \left[\frac{2(\tilde{\mu}_\lambda \omega^2 - 2\chi m_\lambda E_k)}{(\omega^2 + E_k^2 + m_\lambda^2)^2} - \frac{\tilde{\mu}_\lambda}{\omega^2 + E_k^2 + m_\lambda^2} \right], \quad (\text{B19})$$

and in the order B_{\perp}^2

$$\begin{aligned}
m_{\pm}^{(2)} = & \int \frac{d\omega d^2k}{(2\pi)^3} \sum_{\lambda=\pm} \left\{ \left[\frac{1 \pm \lambda}{2} V_{\text{eff}}(\omega, \mathbf{k}) + \frac{2\pi}{m_*} (g_m \pm \lambda g_{m_z}) \right] \left[\frac{16\chi^2 m_{\lambda} E_k^4}{(\omega^2 + E_k^2 + m_{\lambda}^2)^4} \right. \right. \\
& + \frac{4[\chi^2 m_{\lambda} E_k^2 + \tilde{\mu}_{\lambda} (m_{\lambda} \tilde{\mu}_{\lambda} + 4\chi E_k)(E_k^2 + m_{\lambda}^2)]}{(\omega^2 + E_k^2 + m_{\lambda}^2)^3} - \frac{m_{\lambda} (2m_{\lambda} m_{\lambda}^{(2)} + 3\tilde{\mu}_{\lambda}^2 + 2\chi^2) + 12\chi \tilde{\mu}_{\lambda} E_k}{(\omega^2 + E_k^2 + m_{\lambda}^2)^2} \\
& + \left. \frac{4m_x^2 m^2 m_{\lambda}^{(2)} - (\mu_z^{(1)})^2 [m_{\lambda} (E_k^2 + m^2) - 2\lambda m_x m^2]}{4m_x^2 m^2 (\omega^2 + E_k^2 + m_{\lambda}^2)} - \frac{(\mu_z^{(1)})^2 m_{\lambda} (E_k^2 + m_{\lambda} m)}{\lambda m_x m (\omega^2 + E_k^2 + m_{\lambda}^2)^2} \right] \\
& + \left. \left[\frac{1 \mp \lambda}{2} V_{\text{eff}}(\omega, \mathbf{k}) + \frac{2\pi}{m_*} (g_m \mp \lambda g_{m_z}) \right] \frac{(\mu_z^{(1)})^2 [m_{\lambda} (E_k^2 + m^2) - 2\lambda m_x E_k^2]}{4m_x^2 m^2 (\omega^2 + E_k^2 + m_{\lambda}^2)} \right\}, \tag{B20}
\end{aligned}$$

$$\begin{aligned}
\Delta_z^{(2)} = & \int \frac{d\omega d^2k}{(2\pi)^3} \sum_{\lambda=\pm} \frac{\lambda}{2m_x m} \left[\frac{2\mu_z^{(1)} [m(\tilde{\mu}_{\lambda} \omega^2 - 2\chi m_{\lambda} E_k) - 2\chi E_k^3]}{(\omega^2 + E_k^2 + m_{\lambda}^2)^2} - \frac{\mu_z^{(1)} \tilde{\mu}_x^{(1)} (E_k^2 + m^2)}{m_x (\omega^2 + E_k^2 + m_{\lambda}^2)} \right. \\
& + \left. \frac{\mu_z^{(1)} [m(\tilde{\mu}^{(1)} - 2\tilde{\mu}_{\lambda}) + 4\chi E_k] + m_{\lambda} m \Delta_z^{(2)}}{\omega^2 + E_k^2 + m_{\lambda}^2} \right] \left[V_{\text{eff}}(\omega, \mathbf{k}) + \frac{4\pi}{m_*} g_{\Delta_z} \right], \tag{B21}
\end{aligned}$$

where $m_{\pm} = m \pm m_x$, $\tilde{\mu}_{\pm} = \tilde{\mu}^{(1)} \pm \tilde{\mu}_x^{(1)}$, and $m_{\pm}^{(2)} = m^{(2)} \pm m_x^{(2)}$. The energy density (17) expanded up to the second order in B_{\perp} takes the form

$$\begin{aligned}
\mathcal{E} = & \frac{i}{2} \int \frac{d\omega d^2p}{(2\pi)^3} \text{tr} \left\{ [(-\omega - m_0 \eta_3 \tau_3 + D_0) + (-\mu_B B_{\perp} \sigma_3 + B_{\perp} D_1) + B_{\perp}^2 D_2] \left(\tilde{G}_0 + B_{\perp} \tilde{G}_1 + B_{\perp}^2 \tilde{G}_2 \right) \right\} \\
& - (\mu_z, \tilde{\mu}, \tilde{\mu}_z, m^{(2)}, m_z^{(2)}, B_{\perp} \rightarrow 0) \\
\equiv & \frac{i}{2} \int \frac{d\omega d^2p}{(2\pi)^3} \text{tr} \left\{ F_0 \tilde{G}_0 + B_{\perp} (F_0 \tilde{G}_1 + F_1 \tilde{G}_0) + B_{\perp}^2 (F_0 \tilde{G}_2 + F_1 \tilde{G}_1 + F_2 \tilde{G}_0) \right\} \\
& - (\mu_z, \tilde{\mu}, \tilde{\mu}_z, m^{(2)}, m_z^{(2)}, B_{\perp} \rightarrow 0), \tag{B22}
\end{aligned}$$

where

$$F_0 = (-\omega - m_0 \eta_3 \tau_3 + D_0), \quad F_1 = \mu_B \sigma_3 + D_1, \quad F_2 = D_2. \tag{B23}$$

The gap equations in a weak perpendicular magnetic field derived in this Appendix are solved numerically, and the results are presented in Sec. VI.

-
- [1] E. McCann and V. I. Fal'ko, Phys. Rev. Lett. **96**, 086805 (2006).
[2] F. Zhang, H. Min, M. Polini, and A. H. MacDonald, Phys. Rev. B **81**, 041402 (2010).
[3] E. V. Gorbar, V. P. Gusynin, V. A. Miransky, and I. A. Shovkovy, Phys. Rev. B **66**, 045108 (2002).
[4] D. V. Khveshchenko and H. Leal, Nucl. Phys. B **687**, 323 (2004).
[5] O. V. Gamayun, E. V. Gorbar, and V. P. Gusynin, Phys. Rev. B **81**, 075429 (2010).
[6] J. Wang, H. A. Fertig, and G. Murthy, Phys. Rev. Lett. **104**, 186401 (2010).
[7] J. González, Phys. Rev. B **85**, 085420 (2012).
[8] R. Nandkishore and L. Levitov, Phys. Rev. Lett. **104**, 156803 (2010).
[9] The different role of interactions for semimetals with linear and quadratic electron dispersion was recognized in an early work: A.A. Abrikosov and S.D. Beneslavskii, Zh. Eksp. Teor. Fiz. **59**, 1280 (1970) [Sov. Phys. JETP **32**, 4 (1971)]; J. Low Temp. Phys. **5**, 141 (1971).
[10] A. S. Mayorov, D. C. Elias, I. S. Mukhin, S. V. Morozov, L. A. Ponomarenko, K. S. Novoselov, A. K. Geim, and R. V. Gorbachev, Nano Lett. **12**, 4629 (2012).
[11] R. T. Weitz, M. T. Allen, B. E. Feldman, J. Martin, and A. Yacoby, Science **330**, 812 (2010).
[12] F. Freitag, J. Trbovic, M. Weiss, and C. Schönenberger, Phys. Rev. Lett. **108**, 076602 (2012).
[13] J. Velasco Jr., L. Jing, W. Bao, Y. Lee, P. Kratz, V. Aji, M. Bockrath, C. N. Lau, C. Varma, R. Stillwell, D. Smirnov, F. Zhang, J. Jung, and A. H. MacDonald, Nat. Nanotechnol. **7**, 156 (2012).
[14] W. Bao, J. Velasco, F. Zhang, L. Jing, B. Standley, D. Smirnov, M. Bockrath, A. H. MacDonald, and C. N. Lau, Proc. Natl. Acad. Sci. USA **109**, 10802 (2012).
[15] V. P. Gusynin, V. A. Miransky, and I. A. Shovkovy, Phys. Rev. Lett. **73**, 3499 (1994).

- [16] V. P. Gusynin, V. A. Miransky, S. G. Sharapov, and I. A. Shovkovy, Phys. Rev. B **74**, 195429 (2006); I. F. Herbut, *ibid.* **75**, 165411 (2007); J.-N. Fuchs and P. Lederer, Phys. Rev. Lett. **98**, 016803 (2007); M. Ezawa, J. Phys. Soc. Jpn. **76**, 094701 (2007).
- [17] R. Nandkishore and L. Levitov, Phys. Rev. B **82**, 115124 (2010).
- [18] F. Zhang, J. Jung, G. A. Fiete, Q. Niu, and A. H. MacDonald, Phys. Rev. Lett. **106**, 156801 (2011).
- [19] F. Zhang and A. H. MacDonald, Phys. Rev. Lett. **108**, 186804 (2012).
- [20] F. D. M. Haldane, Phys. Rev. Lett. **61**, 2015 (1988).
- [21] J. Martin, B. E. Feldman, R. T. Weitz, M. T. Allen, and A. Yacoby, Phys. Rev. Lett. **105**, 256806 (2010).
- [22] B. E. Feldman, J. Martin, and A. Yacoby, Nat. Phys. **5**, 889 (2009).
- [23] Y. Zhao, P. Cadden-Zimansky, Z. Jiang, and P. Kim, Phys. Rev. Lett. **104**, 066801 (2010).
- [24] S. Kim, K. Lee, and E. Tutuc, Phys. Rev. Lett. **107**, 016803 (2011).
- [25] H. J. van Elferen, A. Veligura, E. V. Kurganova, U. Zeitler, J. C. Maan, N. Tombros, I. J. Vera-Marun, and B. J. van Wees, Phys. Rev. B **85**, 115408 (2012).
- [26] B. M. Hunt, J. I. A. Li, A. A. Zibrov, L. Wang, T. Taniguchi, K. Watanabe, J. Hone, C. R. Dean, M. Zaletel, R. C. Ashoori, and A. F. Young, arXiv:1607.06461.
- [27] M. Kharitonov, Phys. Rev. Lett. **109**, 046803 (2012).
- [28] Y. Barlas, R. Côté, K. Nomura, and A. H. MacDonald, Phys. Rev. Lett. **101**, 097601 (2008).
- [29] D. S. L. Abergel and T. Chakraborty, Phys. Rev. Lett. **102**, 056807 (2009).
- [30] K. Shizuya, Phys. Rev. **79**, 165402 (2009).
- [31] M. Nakamura, E. V. Castro, and B. Dóra, Phys. Rev. Lett. **103**, 266804 (2009).
- [32] E. V. Gorbar, V. P. Gusynin, and V. A. Miransky, Pis'ma Zh. Eksp. Teor. Fiz. **91**, 334 (2010) [JETP Lett. **91**, 314 (2010)]; Phys. Rev. B **81**, 155451 (2010).
- [33] R. Nandkishore and L. Levitov, Phys. Scr. **T146**, 014011 (2012).
- [34] C. Tóke and V. I. Fal'ko, Phys. Rev. B **83**, 115455 (2011).
- [35] E. V. Gorbar, V. P. Gusynin, J. Jia, and V. A. Miransky, Phys. Rev. B **84**, 235449 (2011).
- [36] E. V. Gorbar, V. P. Gusynin, V. A. Miransky, and I. A. Shovkovy, Phys. Rev. B **85**, 235460 (2012).
- [37] M. Kharitonov, Phys. Rev. B **86**, 075450 (2012).
- [38] M. Kharitonov, Phys. Rev. B **86**, 195435 (2012).
- [39] Y. Lemonik, I. L. Aleiner, C. Toke, and V. I. Fal'ko, Phys. Rev. B **82**, 201408(R) (2010); Y. Lemonik, I. Aleiner, and V. I. Fal'ko, *ibid.* **85**, 245451 (2012).
- [40] O. Vafek, Phys. Rev. B **82**, 205106 (2010); V. Cvetkovic, R. E. Throckmorton, and O. Vafek, *ibid.* **86**, 075467 (2012); R. E. Throckmorton and O. Vafek, *ibid.* **86**, 115447 (2012).
- [41] M. Kharitonov, Phys. Rev. B **85**, 155439 (2012).
- [42] P. Maher, C. R. Dean, A. F. Young, T. Taniguchi, K. Watanabe, K. L. Shepard, J. Hone, and P. Kim, Nat. Phys. **9**, 154 (2013).
- [43] F. Freitag, M. Weiss, R. Maurand, J. Trbovic, and C. Schönenberger, Phys. Rev. B **87**, 161402(R) (2013).
- [44] S. S. Pershoguba and V. M. Yakovenko, Phys. Rev. B **82**, 205408 (2010).
- [45] B. Roy and K. Yang, Phys. Rev. B **88**, 241107(R) (2013).
- [46] M. Van der Donck, F. M. Peeters, and B. Van Duppen, Phys. Rev. B **93**, 115423 (2016).
- [47] N. Kheirabadi, E. McCann, and V. I. Fal'ko, Phys. Rev. B **94**, 165404 (2016).
- [48] B. Roy, M.P. Kennett, and S. Das Sarma, Phys. Rev. B **90**, 201409(R) (2014).
- [49] B. Roy, Phys. Rev. B **89**, 201401(R) (2014).
- [50] K. G. Klimenko and R. N. Zhokhov, Phys. Rev. D **88**, 105015 (2013).
- [51] S. Pezzini, C. Cobaleda, B. A. Piot, V. Bellani, and E. Diez, Phys. Rev. B **90**, 121404(R) (2014).
- [52] P. San-Jose, J. L. Lado, R. Aguado, F. Guinea, and J. Fernandez-Rossier, Phys. Rev. X **5**, 041042 (2015).
- [53] M. R. Douglas and N. A. Nekrasov, Rev. Mod. Phys. **73**, 977 (2001).